

Gravitational wave of intermediate-mass black holes in Population III star clusters

Long Wang,^{1,2,3}★ Ataru Tanikawa,⁴ Michiko Fujii³

¹*School of Physics and Astronomy, Sun Yat-sen University, Daxue Road, Zhuhai, 519082, China*

²*CSST Science Center for the Guangdong-Hong Kong-Macau Greater Bay Area, Zhuhai, 519082, China*

³*Department of Astronomy, Graduate School of Science, The University of Tokyo, 7-3-1 Hongo, Bunkyo-ku, Tokyo 113-0033, Japan*

⁴*Department of Earth Science and Astronomy, College of Arts and Sciences, The University of Tokyo, 3-8-1 Komaba, Meguro-ku, Tokyo 153-8902, Japan*

Accepted XXX. Received YYY; in original form ZZZ

ABSTRACT

Previous theoretical studies suggest that the Population III (Pop3) stars tend to form in extremely metal poor gas clouds with approximately $10^5 M_{\odot}$ embedded in mini dark matter halos. Very massive stars can form via multiple collisions in Pop3 star clusters and eventually evolve to intermediate-mass black holes (IMBHs). In this work, we conduct star-by-star N -body simulations for modelling the long-term evolution of Pop3 star clusters. We find that if the mini dark matter halos can survive today, these star clusters can avoid tidal disruption by the galactic environment and can efficiently produce IMBH-BH mergers among a wide range of redshift from 0 to 20. The average gravitational wave event rate is estimated to be $0.1 - 0.8 \text{ yr}^{-1} \text{ Gpc}^{-3}$, and approximately 40 – 80 percent of the mergers occur at high redshift ($z > 6$). The characteristic strain shows that a part of low-redshift mergers can be detected by LISA, TianQin, and Taiji, whereas most mergers can be covered by DECIGO and advanced LIGO/VIRGO/Kagra. Mergers with pair-instability BHs have a rate of approximately $0.01 - 0.15 \text{ yr}^{-1} \text{ Gpc}^{-3}$, which can explain the GW190521-like events.

Key words: methods: numerical – galaxies: star clusters: general – stars: black holes – stars: Population III

1 INTRODUCTION

The formation of super massive black holes (SMBHs) is one key question for understanding the cosmological structure formation. If the massive galaxies grow up via assembly of low-mass ones, the masses of their central SMBHs is also expected to increase via the mergers of binary SMBHs. The $M - \sigma$ and $M_{\text{BH}} - M_{\text{bulge}}$ relations suggest such co-evolution (see Kormendy & Ho 2013, and references therein). The high-precision observation of stellar orbits near the Galactic center suggests an SMBH of $4.28 \times 10^6 M_{\odot}$ (Ghez et al. 1998, 2005, 2008; Gillessen et al. 2009, 2017). Recently, the Event Horizon Telescope detect the emission surrounding a SMBH of $6.5 \times 10^9 M_{\odot}$ at the center of the elliptical galaxy M87 (Event Horizon Telescope Collaboration et al. 2019).

The Ligo-Virgo-KAGRA (LVK) ground-based gravitational wave (GW) detectors have detected a group of stellar-mass black hole (BH) mergers with a chirp mass of up to approximately $100 M_{\odot}$ (Abbott et al. 2019, 2021; The LIGO Scientific Collaboration et al. 2021). The gap between stellar-mass BHs and SMBHs, the intermediate-mass black holes (IMBHs) or the potential seed of SMBHs, with a mass range between $10^3 - 10^5 M_{\odot}$ are still missing conclusive evidence. A recent review of IMBH can be found in Greene et al. (2020).

Considerable efforts have been driven to find the evidence of IMBHs in the extra-galactic environment, including ultraluminous X-Ray sources (ULXs), such as M82 (Kaaret et al. 2001; Matsumoto

et al. 2001; Hopman et al. 2004), spiral galaxy NGC 1313 (Miller et al. 2003), NGC 4395 (Shih et al. 2003), NGC 4559 (Cropper et al. 2004), POX 52 (Barth et al. 2004), NGC 3628 (Strickland et al. 2001), M101 (Kong et al. 2004), Galaxy ESO 243-49 HLX-1 (Farrell et al. 2009; Wiersema et al. 2010; Davis et al. 2011; Lasota et al. 2011; Farrell et al. 2012; Webb et al. 2012), NGC 5408 X-1 (Strohmayer & Mushotzky 2009), NGC 2276 (Mezcua et al. 2015) and many other candidates (e.g., Sutton et al. 2012). IMBHs can also exist in active galactic nuclei (AGN) (e.g., Greene & Ho 2004; Kamizasa et al. 2012; Chilingarian et al. 2018; Mezcua et al. 2018). However, the mass estimation of SMBHs or IMBHs in the extra galactic environment has a large uncertainty. It depends on which disk model is assumed (e.g., Vierdayanti et al. 2006). K rding et al. (2002) suggested that if X-ray sources do not have isotropic emission, but are relativistically beamed, the required BH masses are reduced to stellar mass.

IMBHs might also exist in dense globular clusters (GCs). However, it is also challenging to confidently confirm the existence of IMBHs there. One manner to detect IMBHs is by measuring the rise of line-of-sight velocity dispersion of central stars, such as Hubble Space Telescope (HST) observations of M15 (van der Marel et al. 2002; Gerssen et al. 2002, 2003) and the HST and Keck observations of G1 (Gebhardt et al. 2002, 2005). Nevertheless, it is difficult to distinguish whether it is a IMBH, a group of stellar-mass BHs and NSs, or just a stellar-mass binary BH (BBH) (e.g., Hurley 2007). If BBHs are detected in GCs, the probability of existing an IMBH is small (Leigh et al. 2014). McNamara et al. (2003) analysed the proper motion of

★ E-mail: wanglong8@mail.sysu.edu.cn (Sysu)

HST and performed N -body models. They concluded that there is a weak evidence of IMBH in M15. Baumgardt et al. (2003a) and Baumgardt et al. (2003b) showed that the N -body models of M15 and G1 are consistent with no IMBH. Pooley & Rappaport (2006) indicated that X-rays from G1 cannot distinguish whether it is an IMBH or a low-mass X-ray binary.

A massive GC such as ω -Centauri is one potential candidate to hold an IMBH (Baumgardt 2017). The HST and Gemini GMOS-IFU observations found an increase of central velocity dispersion (Noyola et al. 2008). However, further studies have contradictory results (Anderson & van der Marel 2010a,b). Zocchi et al. (2017) argued that the radial anisotropy can also explain the velocity dispersion profile instead of an IMBH. A following study by using the dynamical model from Baumgardt et al. (2019) also supported this result.

Another series of IMBH detections from the Very Large Telescope (VLT) and HST integrated spectroscopic data show a rise of central velocity dispersion in NGC 6388 (Lützgendorf et al. 2011), NGC 2808 (Lützgendorf et al. 2012), NGC 5286 (Feldmeier et al. 2013) and other GCs (Lützgendorf et al. 2013). However, this evidence is inconclusive. The velocity measurement from individual stars based on the HST and the Wide Field Instrument (WFI) shows no rise of the velocity dispersion at the center of NGC 6388 (Lanzoni et al. 2013).

Using pulsar data, Kızıltan et al. (2017) claimed that an IMBH exists in 47 Tuc GC, and Perera et al. (2017) suggest an IMBH may exist in NGC 6624, depending on orbital eccentricity. Mann et al. (2019) argued that the multi-mass velocity dispersion shows that stellar mass BHs are sufficient to explain the observational data in 47 Tuc GC. The dynamical model from Baumgardt et al. (2019) suggests no evidence of IMBH in NGC 6624. No radio signal of IMBHs has been detected in NGC 2808 (Maccarone & Servillat 2008) and other GCs thus far (the MAVERIC project from Tremou et al. 2018).

Lin et al. (2018) discovered a tidal disruption event in an off-center star cluster of a large lenticular galaxy, where an IMBH might exist with the mass ranging from 5×10^4 to $10^5 M_{\odot}$. Efforts have also been driven to detect IMBH in molecular cloud. The millimetre-wave emission indicates that a massive IMBH might exist in CO-0.40-0.22 (Oka et al. 2017). Several other works are not fully covered here.

Future observations, particularly the GW detection, will accurately measure the masses of BHs and probably find the first strong proof of IMBHs. Space-borne GW detectors, such as LISA (Will 2004; Amaro-Seoane et al. 2022), TianQin (Luo et al. 2016; Fan et al. 2020; Liu et al. 2020), Taiji (Ruan et al. 2020), and DECIGO (Kawamura et al. 2011), can detect the signals of IMBH from a wide region of redshift (z), particularly the seed of SMBH with $z > 10$. The GW lensing of IMBHs can also be detected (Lai et al. 2018). The highly eccentric IMBH-BH merger from Lidov-Kozai (LK) oscillations can also be detected by the ground-based detector like LVK (Fragione & Bromberg 2019). Combining the space-borne GW detectors and ground-base detectors including LVK, Einstein Telescope (Punturo et al. 2010), and Cosmic Explorer (Reitze et al. 2019), the future multiband detectors can provide rich information of GW from IMBHs (Jani et al. 2020),

Moreover, the formation process of IMBHs should be understood, which is also reflected on the properties of GW signals. IMBHs can form via a continual merger of stellar-mass objects in dense stellar systems. In post core-collapse massive star clusters where the central number density $> 10^5 \text{ pc}^{-3}$, the continual mergers of stellar-mass BHs can generate IMBH with $M > 10^3 M_{\odot}$ (e.g., Miller & Hamilton 2002; Gültekin et al. 2004; Giersz et al. 2015; Rizzuto et al. 2021; Mapelli et al. 2021, 2022). With a higher density, the runaway

mergers can rapidly generate IMBH (e.g., Mouri & Taniguchi 2002; Giersz et al. 2015). Massive IMBHs and the seeds of super massive black holes (SMBHs) can form in the circumnuclear giant HII region (e.g., Taniguchi et al. 2000) and in nuclear star clusters (e.g., Antonini et al. 2019; Fragione & Silk 2020; Kroupa et al. 2020; Fragione et al. 2022b; Rose et al. 2022), where a strong gravitational potential from the galaxy can prevent the escape of compact remnants due to natal kick after supernovae, dynamical ejection after few-body interactions or dynamical recoil kicks due to asymmetric GW.

In an AGN disk around SMBH, IMBH can form via mergers of stars (McKernan et al. 2012, 2014). In addition, IMBHs and SMBHs may also form via the direct collapse of metal-poor giant gas where the gas cloud undergoes gravitational collapse without the formation of stars at the galactic center (e.g., Mayer et al. 2010, 2015).

In a starburst star-forming region with a high central density, the continual mergers of massive stars can generate very massive stars (VMS), which subsequently evolve to IMBHs (e.g., Portegies Zwart & McMillan 2002; Portegies Zwart et al. 2004, 2006; Freitag et al. 2006; Kremer et al. 2020; González et al. 2021). A VMS with $Z < 10^{-3}$ does not undergo pair-instability supernovae and can directly collapse to an IMBH (Spera & Mapelli 2017).

The hierarchical hydrodynamic model of population III (Pop3) star formation from Sakurai et al. (2017) suggested that VMSs can also form in Pop3 star clusters and result in IMBHs. There are a few aspects that suggest Pop3 star clusters might be an environment that contain IMBHs. First, the formation times of SMBH seeds and of Pop3 stars overlap. Second, the extremely metal-poor gas tends to result in a top-heavy initial mass function (IMF; Stacy et al. 2016; Chon et al. 2021; Latif et al. 2022), where a large fraction of Pop3 stars is massive and can either merge to form VMSs or become BHs. Third, unlike the metal-rich stars, the final mass of the BHs formed from the death of a VMS can be considerably higher without a significant wind mass loss. Fourth, Pop3 star clusters form inside mini dark matter halos (e.g., Skinner & Wise 2020). The halos can protect the clusters from tidal disruptions. Hence, IMBH-BH or BBH mergers can continually occur inside Pop3 star clusters across a wide redshift region.

In previous studies, Sakurai et al. (2017) investigated the possibility to form VMSs in Pop3 star clusters, but did not follow the long-term evolution of the stars. Liu et al. (2021) studied small Pop3 star clusters, and the dynamical effects are not sufficiently pronounced to form VMSs. Reinoso et al. (2018) generated a group of low-mass star-cluster models with minimum $Z = 0.0001$ to study the collision rate depending on the cluster's initial conditions. Tanikawa et al. (2022) studied the contribution of BBH mergers from all three populations of stars.

In this work, we investigate the long-term evolution of Pop3 star clusters under mini dark matter halos in detail by performing star-by-star N -body simulations with extremely metal-poor stars and IMBH-BH GW mergers. Section 2 introduces the numerical method and the initial condition of the N -body simulations. Section 3 shows the formation of VMSs and IMBHs, the influence of dark matter halos on the long-term evolution of Pop3 star clusters, and the properties of BBH, IMBH-BH, and IMBH-star mergers. In Section 4, we discuss how the uncovered physical mechanisms affect the predictions of GW events. In Section 5, we draw the conclusion.

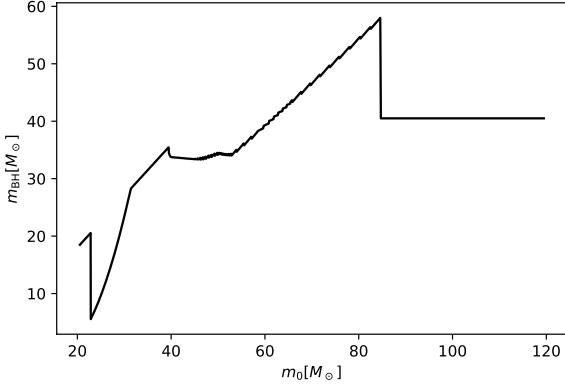


Figure 1. Final BH masses (m_{bh}) vs. zero-age main-sequence masses (m_0) for stars with $Z = 2 \times 10^{-10}$, evolved using BSEEMP.

2 METHOD

2.1 PeTar code

In this work, we used the high-performance N -body code `PETAR` (Wang et al. 2020b) to conduct simulations of Pop3 star clusters. The code was developed based on the particle-tree and particle-particle algorithm (Oshino et al. 2011) under the Framework for Developing Particle Simulator (FDPS; Iwasawa et al. 2016, 2020). The slow-down algorithmic regularization method (Wang et al. 2020a) was implemented to ensure an accurate and efficient treatment of binary orbital evolution and close encounters. `GALPY` (Bovy 2015) was implemented to address the external potential.

2.2 bseEmp

The single and binary stellar evolution codes based on the fast population synthesis method, `SSE` and `BSE`, have been frequently used for N -body simulations of star clusters (Hurley et al. 2000, 2002; Banerjee et al. 2020). In this work, we used an extended version, `BSEEMP` (Tanikawa et al. 2020), which includes the fitting formula for stars formed in extremely metal-poor environments. Thus, we were able to trace the stellar wind mass loss and the BH formation of Pop3 stars with the minimum metallicity, $Z = 2 \times 10^{-10}$.

The limitations of the fitting formula we adopted are clarified here. Tanikawa et al. (2020, 2021b) constructed the fitting formula, referring to one-dimensional hydrodynamics simulation of 8 - $1280 M_{\odot}$ stars by the `HOSHI` code (Takahashi et al. 2016, 2019, 2018; Yoshida et al. 2019). For the high-mass limit, we can correctly follow stellar evolution up to $1280 M_{\odot}$. Moreover, we safely trace the stellar evolution and dynamics of $m > 1280 M_{\odot}$ stars, say stars with at least several $10^3 M_{\odot}$ for the following reason. Extrapolating the fitting formula, we find that the maximum radii of stars can be written as $R/10^4 R_{\odot} = (m/1280 M_{\odot})^{1.2}$ up to a few $10^4 M_{\odot}$. The maximum radii gradually increase with increasing mass. Thus, we do not overestimate nor underestimate the merger rate of $m > 1280 M_{\odot}$ stars in our simulations. At the low-mass limit ($m < 8 M_{\odot}$), we approximate Pop3 star evolution as $Z = 0.0001$ star evolution as constructed by Hurley et al. (2000). As BHs, remnants of $m \gtrsim 20 M_{\odot}$ stars, control the dynamics of the Pop3 star clusters we examined, this approximation has little impact on our results.

For supernova model, we adopt the Fryer’s rapid model (Fryer et al. 2012) with the modification of pair instability supernova (Heger et al. 2003) and pulsational pair instability supernova (Woosley 2017) modeled by Belczynski et al. (2016) (see also Banerjee et al. 2020).

Figure 1 shows the masses of BHs depending on the zero-age main-sequence masses of Pop3 stars with the upper mass limit of $150 M_{\odot}$ and $Z = 2 \times 10^{-10}$ via the pure single stellar evolution. We obtained the data by using the standalone code `BSEEMP` (single stellar evolution is also included). Stars with $m_0 = 85$ - $121 M_{\odot}$ (helium core masses of 45 - $65 M_{\odot}$) cause pulsational pair-instability supernovae, and leave behind approximately $40 M_{\odot}$ BHs. When $m_0 > 121 M_{\odot}$ (or helium core masses are $> 65 M_{\odot}$), no BHs form because of pair-instability supernova.

The binary stellar evolution and dynamically driven formation of binaries can produce BHs with masses in the pair-instability mass gap. Here, we define the pair-instability mass gap as the mass range from 60 to $121 M_{\odot}$, and name BHs within this mass gap as “pair-instability BHs” (PIBH). First of all, we consider the pair-instability mass gap as the mass range in which no BHs are present if all BH progenitors evolve as single stars. The upper bound is the BH formed from the minimum naked helium star ($135 M_{\odot}$) which overcomes a pair-instability supernova explosion and directly collapses to a BH. The lower bound is $m_{\text{bh}} \approx 60 M_{\odot}$. This is larger than the generally discussed pair-instability mass gap lower limit ($\sim 40 M_{\odot}$). Such BHs can be formed from stars with massive hydrogen envelopes and helium cores with mass less than $\sim 45 M_{\odot}$, because these stars can avoid pulsational pair instability supernovae due to small helium core masses. Thus, based on this stellar evolution model of `BSEEMP` for Pop3 stars, we expect that BHs with masses between 40 – $60 M_{\odot}$ can form efficiently.

2.3 Initial conditions

The hydrodynamic simulations from Sakurai et al. (2017) show that the center of Pop3 star clusters tends to have a high density, which can trigger the hierarchical mergers and VMSs formation subsequently. For an individual star cluster, the initial density distribution is irregular and is strongly affected by stochastic fluctuations. However, the cluster evolves into virial equilibrium state in the crossing time,

$$T_{\text{cr}} = \sqrt{\frac{r_{\text{h}}^3}{GM_{\text{sc}}}}, \quad (1)$$

where r_{h} is the half-mass radius and M_{sc} is the mass of the star cluster. After T_{cr} , the morphology of the cluster becomes spherical or elliptical. Meanwhile, gas is removed by feedback from massive stars, including radiation, stellar winds and supernovae. We start our simulation in the virial equilibrium without gas dynamics. The initial M_{sc} was fixed to $10^5 M_{\odot}$, following a similar mass of Model A in Sakurai et al. (2017). The initial $r_{\text{h}} = 1$ pc, which is a typical value for observed star clusters. To cover the different initial central density possibilities, we applied the Michie (1963)-King (1966) model where the central concentration can be adjusted by modifying the parameter W_0 , which indicates the ratio between the core radius (r_{c}) and the tidal radius (r_{t}). We investigated three values of W_0 : 6, 9, and 12. The corresponding r_{c} values are 0.30, 0.06, 0.01 pc, respectively. The commonly assumed Plummer model (Plummer 1911) for describing the density profile of star clusters is close to the case when $W_0 = 6$. When $W_0 = 12$, the model with a few thousand stars has the highest density concentration.

The hydrodynamic models of Pop3 star formation suggest a top-heavy IMF (Stacy et al. 2016; Chon et al. 2021; Latif et al. 2022) with the power index being approximately -1.0 . We assumed a single power-law IMF with the number of stars per mass bin following a linear scale.

$$\xi(m) \propto m^{-1.0}, m_{\text{imf, min}} < m < 150 M_{\odot}. \quad (2)$$

Compared to the canonical IMF with the index of -2.35 (e.g., [Kroupa 2001](#); [Chabrier 2003](#)), the top-heavy IMF results in a considerably larger fraction of massive stars. Thus, we expect the formation of VMSs to be common and a large number of stellar-mass BHs to form. The cluster eventually evolves into a "dark cluster" ([Banerjee & Kroupa 2011](#)) where most members are BHs. Thus, the cluster cannot be detected via electromagnetic observations. The power index of the IMF has a large uncertainty. We simply used -1.0 to represent the effect of the top-heavy IMF. As the mass range of the IMF is still unclear, we fixed the maximum value to be the classical value of $150 M_{\odot}$. For $W_0 = 12$, we investigated three values of $m_{\text{imf},\text{min}}$: 0.1, 1, and $10 M_{\odot}$. For other W_0 , we adopted $m_{\text{imf},\text{min}}$ to be $1 M_{\odot}$.

The hydrodynamical models show that massive stars tend to form in the center of dense clouds. [Plunkett et al. \(2018\)](#) showed that primordial mass-segregation may exist in extremely young embedded clusters. Thus, we considered the cases with and without primordial mass-segregation for different W_0 and $m_{\text{imf},\text{min}} = 1 M_{\odot}$. The metallicity of stars was fixed to be 2×10^{-10} .

It is unknown what the real conditions of the mini dark matter halo are where Pop3 star clusters form. We assumed a [Navarro et al. \(1996\)](#) (NFW) dark matter halo with the potential:

$$\Phi = -\frac{GM_{\text{vir}}}{r[\log(1+C) - C/(1+C)]} \log\left(1 + \frac{r}{r_s}\right), \quad (3)$$

where M_{vir} , C , and r_s are virial mass, concentration, and scale radius, respectively. The virial radius, $r_{\text{vir}} = cr_s$. To determine the three parameters of the NFW profile, we consider two cases. In the first case, NFWden, we adopted $M_{\text{vir}} = 4 \times 10^7 M_{\odot}$ and $r_{\text{vir}} = 280$ pc, referring to those in model A from [Sakurai et al. \(2017\)](#). We assumed the star clusters formed at redshift, $z = 20$. The initial concentration is unknown for such redshift. Based on the recently high-resolution Uchuu cosmological simulation ([Ishiyama et al. 2021](#)), for a low-mass dark matter halo ($10^9 M_{\odot}$), $C = 14 - 15$ at $z = 0$, which is similar to that of the present-day Milkyway dark matter halo. For the Milkyway halo, $C = 13.1$ ([Gómez et al. 2010](#)) or 15.3 ([Bovy 2015](#)) depending on models. With no data of C for a lower-mass dark matter halo at $z = 20$, we estimate the value as $C(z) = C/(1+z) \approx 0.728571$, assuming $C = 15.3$. In Section 3.2, we discuss the influence of C on the long-term evolution of Pop3 star clusters. In this work, we did not include a time-dependent dark matter halo as that of [Sakurai et al. \(2017\)](#). We aimed to confirm that the existence of dark matter halos can prevent the disruption of Pop3 star clusters. Thus, although the setup of NFWden was an approximation, it was sufficient for the purpose of this work.

For comparison, we set up another dark matter halo (NFWstd). In this halo, the M_{vir} and C are the same as those in the NFWden halo, but r_{vir} is calculated based on the cosmological evolution of dark matter halos described by [Wechsler et al. \(2002\)](#) [Zhao et al. \(2003\)](#), and [Gómez et al. \(2010\)](#):

$$r_{\text{vir}}(z) = \left(\frac{3M_{\text{vir}}(z)}{4\pi\Delta_{\text{vir}}(z)\rho_c(z)}\right)^{1/3}, \quad (4)$$

with

$$\Delta_{\text{vir}}(z) = 18\pi^2 + 82[\Omega(z) - 1] - 39[\Omega(z) - 1]^2, \quad (5)$$

from [Bryan & Norman \(1998\)](#). Here the critical density,

$$\rho_c(z) = \frac{3H^2(z)}{8\pi G}, \quad (6)$$

the normalized mass density of the universe is:

$$\Omega(z) = \left(\frac{H_0}{H(z)}\right)^2 \Omega_M(1+z)^3, \quad (7)$$

Table 1. The initial conditions of star clusters. The first column shows the name prefixes of the models, The suffixes '-std', '-den' and '-nodm' refer to the sets of dark matter halos, NFWstd, NFWden and NoDM, respectively. Each model has 30 simulations with different random seeds for generating initial distribution of stars. The second column shows the averaged initial number of stars.

Name prefix	$\langle N \rangle$	W_0	Mass segregation	$m_{\text{imf},\text{min}}$
Short-term (up to 20 Myr) NFWstd (-std) and NFWden (-den)				
sw6imf1	3369	6	no	1
sw9imf1	3369	9	no	1
sw12imf1	3369	12	no	1
sw6imf1ms	3369	6	yes	1
sw9imf1ms	3369	9	yes	1
sw12imf1ms	3369	12	yes	1
sw12imf01	4882	12	no	0.1
sw12imf10	1935	12	no	10
Long-term (up to 12 Gyr) NFWstd, NFWden and NoDM (-nodm)				
lw6imf1		6	no	1
lw9imf1		9	no	1

and

$$H(z) = H_0 \sqrt{\Omega_{\Gamma}(z+1)^4 + \Omega_M(z+1)^3 + \Omega_{\Lambda}}, \quad (8)$$

where H_0 is the present-day Hubble constant, and Ω_{Γ} , Ω_M and Ω_{Λ} are the radiation density, mass density and energy density of the universe at the present day. We adopted $H_0 = 70(\text{km s}^{-1})\text{Mpc}^{-1}$, $\Omega_{\Gamma} = 0$, $\Omega_M = 0.3$, and $\Omega_{\Lambda} = 0.7$. With the same value of M_{vir} as that of NFWden, the estimated $r_{\text{vir}} \approx 522$ pc, approximately twice of that in NFWden. Thus, the mini dark matter halo of [Sakurai et al. \(2017\)](#) is denser.

For each combination of W_0 , mass segregation, and $m_{\text{imf},\text{min}}$, we performed two models with the NFWstd or the NFWden halos for up to 20 Myr. As the hierarchical mergers of massive stars occurs in a short time, this is sufficient to investigate the formation of IMBH. Moreover, we conducted another group of long-term models, where $W_0 = 6$ and 9 , no mass segregation, and $m_{\text{imf},\text{min}} = 1 M_{\odot}$ were combined with NFWstd, NFWden, and no dark matter halo (NoDM). All models are summarized in Table 1. For each model, as N was small, we performed 30 simulations with different random seeds for generating the initial masses, positions, and velocities of stars to avoid the stochastic effect.

3 RESULTS

3.1 Formation of VMS and IMBH

We investigated the formation of VMSs via hierarchical mergers. Figure 2 shows the number of mergers (n_{merge}) and the maximum final masses of mergers ($m_{f,\text{max}}$) (within 20 Myr) for all short-term models. All mergers with BHs were excluded. Two distinguishable groups of models can be observed: the models with $W_0 = 6$ have almost no mergers and most of their $m_{f,\text{max}}$ are below $50 M_{\odot}$, whereas other models with $W_0 = 9$ and 12 have approximately 4 – 6 mergers and their $m_{f,\text{max}}$ have a wide distribution from 100 to $1300 M_{\odot}$ with an average value approximately $500 M_{\odot}$. Thus, the density profile has the largest impact on the merger rate and the formation of VMSs, whereas primordial mass segregation and $m_{\text{imf},\text{min}}$ have almost no influence. The distribution of $m_{f,\text{max}}$ for the models where VMSs

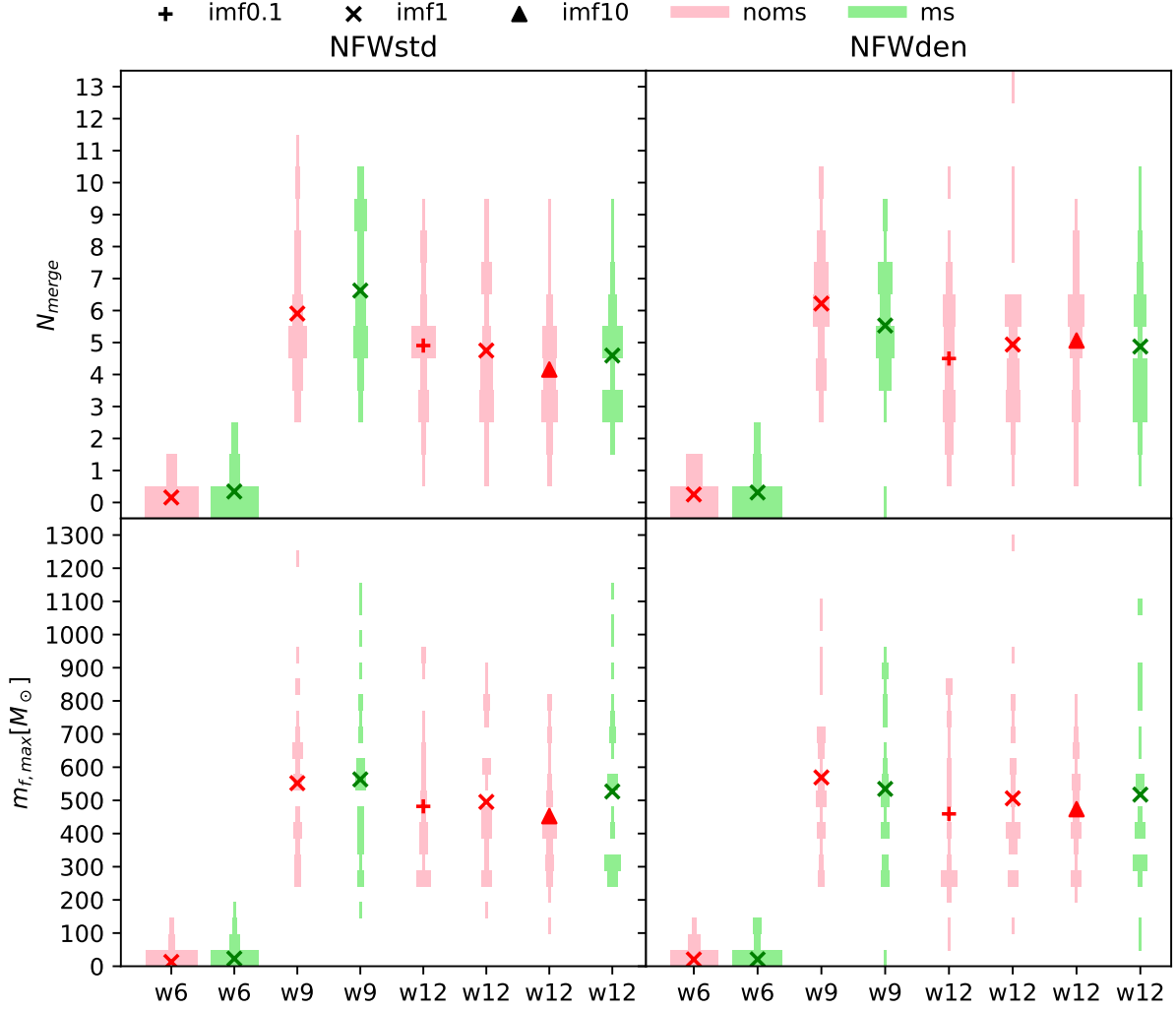


Figure 2. Average numbers of stellar mergers (n_{merger}) and maximum final masses $m_{f,\text{max}}$ of massive stars for each short-term models. Symbols indicate the average values among the 30 simulations of each model, and the width of boxes represents the number fraction of models within the values of the y-axis, similar to a histogram. The bin of the boxes for $m_{f,\text{max}}$ is $50 M_{\odot}$. The colors indicate whether the model has primordial mass segregation; the shapes of symbols represent different $m_{\text{imf},\text{min}}$.

form displays no clear tendency due to the low number of samples (30 samples per model).

As a massive star has a short lifetime and strong stellar wind within a few Myr, the multiple mergers must occur in a short time to successfully produce a VMS. Figure 3 shows an example of multiple mergers in one simulation of the model w12imf1ms-den. Within 2 Myr, a VMS forms after 7 mergers. The final mass reaches above $1000 M_{\odot}$. This is consistent with the prediction of hydrodynamic models from Sakurai et al. (2017).

To understand how the central density affects the merger rate, we calculated the two-body relaxation time ($t_{\text{rx}10}$) within the 10% Lagrangian radii, inelastic encounter rate (f_{ie}), and collision rate (f_{coll}) for different W_0 in Table 2. The sw6imf1, sw9imf1 and sw12imf1 models are used for the calculation. All values were evaluated based on the initial condition.

We used the formula for the two-body relaxation time at the half-mass radius in a equal-mass system (Spitzer 1987), but replaced all

quantities corresponding to the 10% Lagrangian radius (r_{10}):

$$t_{\text{rx}10} = 0.138 \frac{N_{r10}^{1/2} r_{10}^{3/2}}{m_{10} G^{1/2} \ln \Lambda}, \quad (9)$$

where n_{10} and m_{10} are the number of stars and the average mass within r_{10} , respectively. Here the coefficient 0.138 might not be correct for r_{10} , but we use it as an approximation.

f_{ie} is calculated by including the gravitational focusing, following Eq. 7.194 of Binney & Tremaine (1987) (see also Hills & Day 1976):

$$f_{\text{ie}} = 4\sqrt{\pi} n_{10} \sigma_{10} \left(r_{\text{coll}}^2 + \frac{Gm}{\sigma_{10}^2} r_{\text{coll}} \right) \quad (10)$$

where σ_{10} is the velocity dispersion within r_{10} , and r_{coll} is the stellar radius of the star. Similar to $t_{\text{rx}10}$, here we adopted the physical quantities referring to r_{10} to calculate f_{ie} .

f_{coll} represents the collision driven by the dynamically formed binaries via the three-body channel, following the definition in Porte-

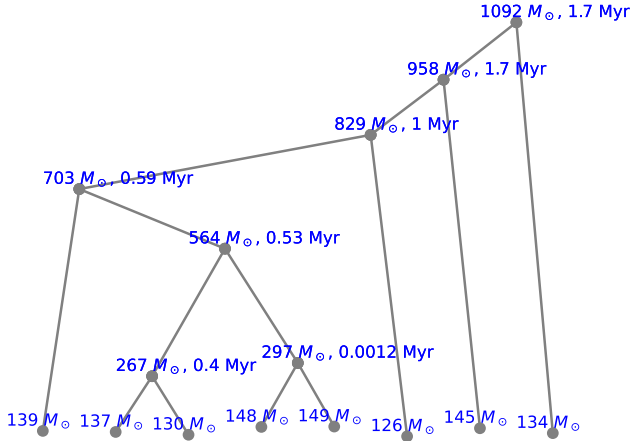


Figure 3. Merger tree for the formation of a VMS in the model msw12m1-den. The masses and merging times of seeds and mergers are shown. All stars in the merger tree are main-sequence stars.

gies Zwart & McMillan (2002):

$$f_{\text{coll}} = 1 \times 10^{-3} f_c \frac{n_{10}}{t_{\text{rx}10}} \quad (11)$$

where f_c is the effective fraction of dynamically formed binaries that produce a collision. We assumed f_c to be 1 for simplicity. Portegies Zwart & McMillan (2002) use the number density and relaxation time at the half-mass radius, but they were the same for different W_0 . Thus, we used r_{10} instead to represent the properties close to the cluster center.

Table 2 suggests that the inelastic encounter is not the major channel that produces mergers as the rate is extremely low. The mergers of dynamically formed binaries well explain our result. For $W_0 = 6$, $f_{\text{coll}} \approx 0.48 \text{ Myr}^{-1}$, whereas for $W_0 = 9$ and 12, $f_{\text{coll}} \geq 1.6 \text{ Myr}^{-1}$. The collision time shown in Figure 3 confirms this estimation.

We also counted the number of hyperbolic mergers driven by inelastic encounters and dynamically binary mergers for all short-term models. The results are 115 and 1906, respectively. Mergers with BHs were excluded. Thus, the dynamically binary mergers are indeed the major contribution.

Figure 3 suggests that the major sources to grow up VMSs are stars with zero-age main-sequence mass above $100 M_\odot$. Thus, it is reasonable that $m_{\text{imf},\text{min}}$ has almost no influence on the formation of VMSs.

The mass segregation time is

$$t_{\text{ms}} \approx \frac{m_{10}}{m_{\text{ms}}} t_{\text{rx}10}, \quad (12)$$

where m_{ms} is the mass of the mass-segregated star. As $t_{\text{rx}10} \leq 0.22 \text{ Myr}$ for $W_0 = 6$ and 9, all stars with mass above $100 M_\odot$ sink into the center shortly after formation. Thus, the merger rate is also independent of primordial mass segregation.

The dark matter halo has no influence as it has a weak impact on the central potential and affects the collisions within 2 Myr. We expect that the dark matter halo can trap the escaped stars and can prevent the expansion of the star cluster due to long-term dynamical evolution, driven by the central binary heating. We discuss this in the next section.

Once a VMS forms, an IMBH can form via three modes:

- S-mode: a VMS directly evolves to an IMBH as a result of

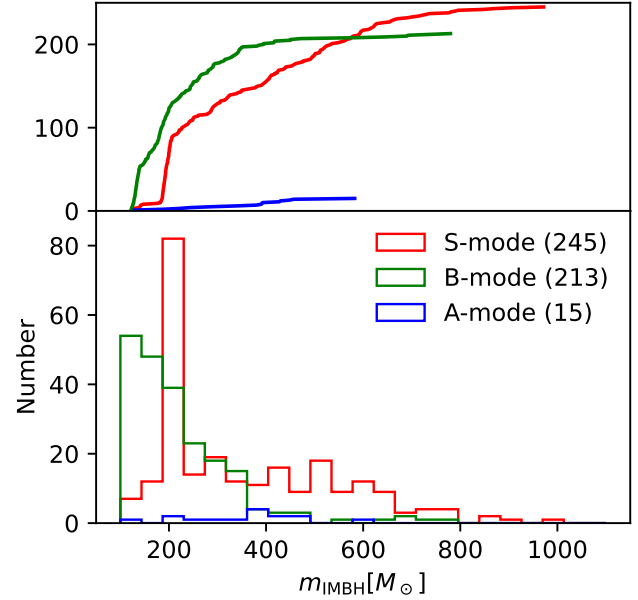


Figure 4. Mass spectrum of IMBHs from three formation modes. The upper panel shows the cumulative distribution, and the bottom panel shows the histogram. All short-term models with $W_0 = 9$ and 12 are included. The minimum mass limit of IMBH is $121 M_\odot$, above the pair-instability supernovae mass gap. The number of formed IMBHs for each mode is shown in the legend.

stellar evolution. For example, the VMS shown in Figure 3 evolves to a first asymptotic giant branch star (FAGB) with $877 M_\odot$. Then, it becomes an IMBH with $789 M_\odot$ at 3.17 Myr. The wind mass loss reduces its mass during stellar evolution.

- B-mode: a VMS evolves to an IMBH in a binary system. Mass transfer may occur between the two binary members. The VMS evolves to a main-sequence naked helium star (HeMS), and then becomes an IMBH.
- A-mode: a VMS can be accreted by a low-mass BH in a VMS-BH binary system and eventually form an low-mass IMBH. During this process, a large fraction (roughly half) of the VMS mass is lost.

$m_{\text{f,max}}$ shows no intrinsic difference among models with $W_0 = 9$ and 12. Thus, we collected all data of formed IMBHs in all these models for better statistical analysis. Figure 4 shows the mass spectrum of formed IMBHs from the three modes. We set the minimum mass limit for IMBHs to be $121 M_\odot$, which is the upper limit of the pair-instability supernovae mass gap. The S-mode and the B-mode contribute equally to the number of IMBHs, while a few IMBHs form from the A-mode. The S-mode produces more massive IMBHs than the B-mode. There is a peak around $200 M_\odot$ in the S-mode, mostly from a massive star undergoing only one merger, which more commonly occurs compared to hierarchical mergers. The A-mode only contributes to a few IMBHs with masses below $500 M_\odot$, except one case of $582 M_\odot$.

Three events in the A-mode are IMBH-VMS mergers, where the masses of the progenitor BHs are already above $121 M_\odot$. Table 3 shows the data for the three IMBH-VMS mergers. The formed IMBH with $582 M_\odot$ had the progenitor VMS of $833 M_\odot$. The binary is circularized before merging. Other two mergers have high eccentric orbits.

Table 2. Number of stars (n_{10}), average density (ρ_{10}), relaxation time (t_{rx10}), inelastic encounter rate (f_{ie}) and collision rate (f_{coll}) calculated within the 10 % Lagrangian radii for the initial conditions of sw6imf1, sw9imf1, and sw12imf1 models. The errors are the standard derivation evaluated from the 30 simulations of each model.

Model	W_0	$n_{10} [\text{pc}^{-3}]$	$\rho_{10} [M_{\odot} \text{pc}^{-3}]$	$t_{rx10} [\text{Myr}^{-1}]$	$f_{ie} [\text{Myr}^{-1}]$	$f_{coll} [\text{Myr}^{-1}]$
sw6imf1	6	343 ± 24	6.3e+04 ± 9.4e+03	0.72 ± 0.072	3.01e-05 ± 3.91e-06	0.48 ± 0.047
sw9imf1	9	331 ± 15	1e+06 ± 1.9e+05	0.18 ± 0.018	3.92e-04 ± 7.18e-05	1.8 ± 0.2
sw12imf1	12	322 ± 22	6.9e+05 ± 2.5e+05	0.22 ± 0.037	2.62e-04 ± 8.80e-05	1.6 ± 0.31

Table 3. IMBH-VMS mergers in short-term models. Columns show merge times (t_f), semi-major axes (a), eccentricities (e), masses of primary members (IMBHs; m_{imbh}), masses of secondary members (VMSs; m_{vms}), and the final masses of IMBHs (m_f), respectively.

t_f [Myr]	$a [R_{\odot}]$	e	$m_{imbh} [M_{\odot}]$	$m_{vms} [M_{\odot}]$	$m_f [M_{\odot}]$
2.25	2747.1	0.99546	250	413	457
2.74	1906.5	3.389e-07	166	833	582
2.54	10980.9	0.99756	131	415	338

3.2 Long-term evolution

The short-term models suggest that IMBHs form at early times due to the formation of VMSs. Hereafter we analyze the long-term evolution of Pop3 star clusters and the GW mergers under the influence of mini dark matter halos. Figure 5 compares the evolution of r_h , r_c , and escape velocity ($v_{esc,sc}$) for the long-term models. Here $v_{esc,sc}$ is estimated by only including the gravitational potential from stars. Without a dark matter halo, the NoDM clusters expand fast for the first 1000 Myr. r_c reaches approximately 5 pc at 12 Gyr. In contrast, models with dark matter halos can keep r_h within 10 pc during the long-term evolution. The strong stellar winds from massive stars cause an fast expansion for the first 100 Myr, which also reduces $v_{esc,sc}$ significantly.

Stars escape from clusters via two mechanisms: tidal evaporation and ejection by binaries in the cluster centre. When the clusters evolve in the galactic potential (which is not included in our models), stars in the halo of clusters feel strong tidal forces and continue escaping. Thus, the noDM models are difficult to survive due to tidal evaporation. However, when a dark matter halo exists, its strong gravitational potential significantly increases the escape velocity of stars; thus, the tidal evaporation process is suppressed. Models with dark matter halos in our simulations can survive till today due to the "protection" of dark matter halo. Thus, we expect that the mergers between stellar mass BHs and IMBHs can continue until today in the long-existed Pop3 star clusters.

Although we only included two models of dark matter halos in our simulations, we can estimate the effect of NFW dark matter halos in general by evaluating the additional central escape velocity ($v_{esc,halo}$) provided by the halo. Based on Equation 3,

$$v_{esc,halo} = \sqrt{[\Phi(\infty) - \Phi(0)]} \\ = \sqrt{\frac{GM_{vir}}{r_s [\log(1+C) - C/(1+C)]}}. \quad (13)$$

For the NFWden and NFWstd halos, the corresponding values are approximately 61 and 45 pc Myr⁻¹, respectively. $v_{esc,sc}$ from star clusters are below 15 pc Myr⁻¹ as shown in Figure 5. As $v_{esc,halo}$ is more than twice $v_{esc,sc}$, stars are difficult to escape under the dark matter halos.

$v_{esc,halo}$ depends on M_{vir} and r_s in a simple manner. The depen-

dence on C is not intuitive. Figure 6 shows how $v_{esc,halo}$ depends on C when M_{vir} and r_{vir} are fixed ($4 \times 10^7 M_{\odot}$ and 522 pc referring to values of the NFWstd halo, respectively). When C increases from 0.5 to 16.5, $v_{esc,halo}$ decreases and then increases. The minimum value (40 pc Myr⁻¹) appears at $C \approx 2.13$. This value is slightly below that of the NFWstd halo in our simulations and is considerably larger than $v_{esc,sc}$ of star clusters. Thus, our result is not strongly affected by the choice of C .

The total escape velocity (v_{esc}) affects the GW merger rate. The orbit of a tight binary in the center of a star cluster shrinks via three-body interactions. However, when a becomes smaller, the center-of-mass of the binary gain a larger kinetic energy. Finally the binary is ejected if not merged. The minimum a that triggers the ejection depends on v_{esc} as (Miller & Hamilton 2002; Mapelli et al. 2021):

$$a_{ej} \propto \frac{\langle m \rangle^2 m_1 m_2}{(m_1 + m_2)^3 v_{esc}^2} \quad (14)$$

where m_1 , m_2 , and $\langle m \rangle$ are the masses of two components of the binary and the average stellar mass of the cluster, respectively. As the GW merger timescale strongly depends on a , a larger v_{esc} results in a higher possibility of GW mergers inside clusters. Therefore, dark matter halos help to prevent the disruption of Pop3 star clusters and also increases the merger rate of GW.

3.3 IMBH-BH mergers

Due to the top-heavy IMF, most members in the survival star clusters under the dark matter halo are BHs. Thus, even the clusters may still exist today in the Galaxy, they cannot be detected by the electromagnetic observations. This is similar to the "dark clusters" discussed in Banerjee & Kroupa (2011). If the clusters have the high central density like that from Sakurai et al. (2017) and the models with $W_0 = 9$ and 12, we expect that the existing IMBH may interact with stellar-mass BH and generate GW signals. The upper panel of Figure 7 shows m_f of all mergers of BHs and IMBHs for the long-term models. The lower panel shows the normalized cumulative distribution of merger time. A large fraction of mergers (0.4 – 0.8) occurs at the first 1 Gyr evolution for all models, because of a high central density. As r_c increases (see Figure 5), the merger rate decreases, but mergers continue until the end of simulations (12 Gyr). This suggests that IMBH-BH and BBH mergers can be detected at all redshift regions. The merger time distribution follows the standard distribution in which $\propto t^{-1}$ (e.g., Totani et al. 2008).

Figure 8 shows the m_1 and m_2 of each merger and the normalized cumulative distribution of the mass ratio q . With IMBHs ($W_0 = 9$), a large fraction of mergers (0.4 – 0.8) has $q < 0.2$, which is larger than the definition of intermediate mass-ratio inspirals (IMRI) discussed in general ($10^{-5} - 10^{-2}$). A denser dark matter halo results in more low- q mergers. For models without IMBHs, the dark matter halo also helps to increase the fraction of low- q mergers. Few massive BBH mergers have binary members with a mass above $200 M_{\odot}$ each. The

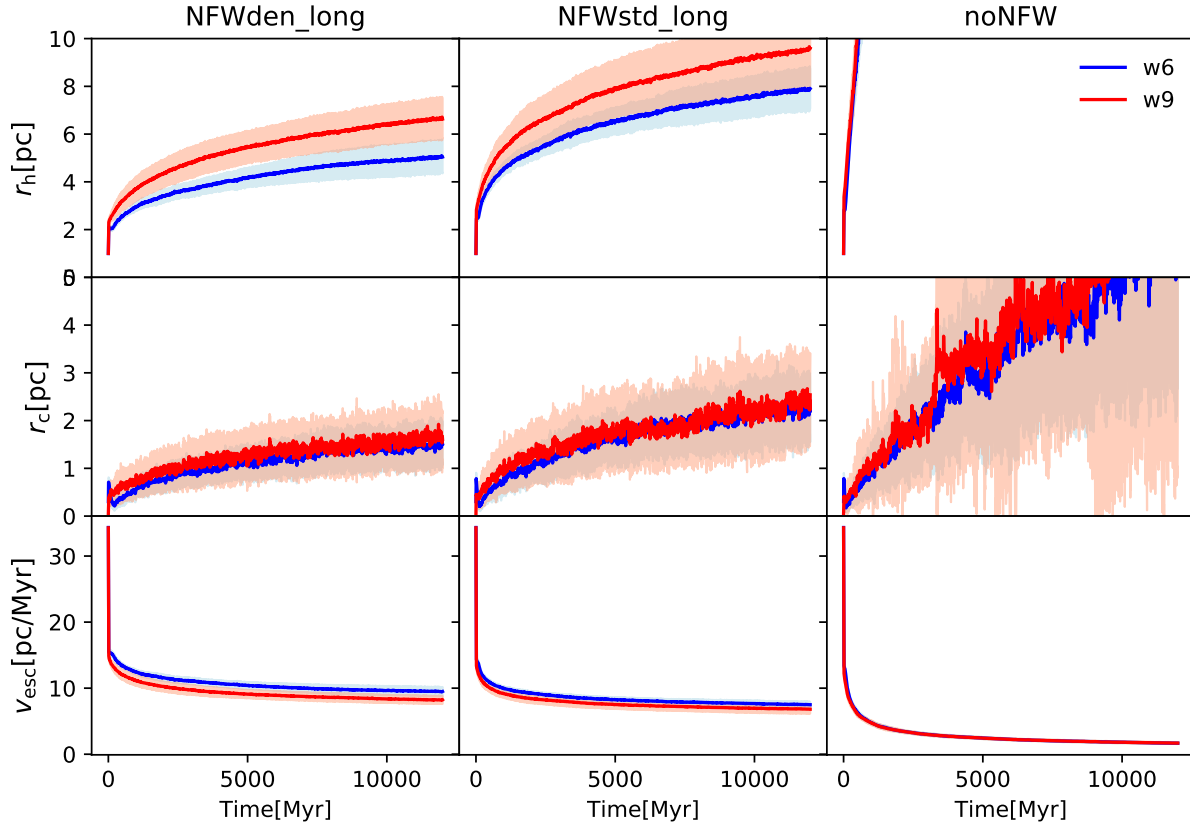


Figure 5. Evolution of the half-mass radii (r_h), core radius (r_c), and escape velocity only from stars ($v_{esc,sc}$) for the long-term models. The solid curves are the average of 30 simulations for each model. The area of light colors indicates the standard derivative.

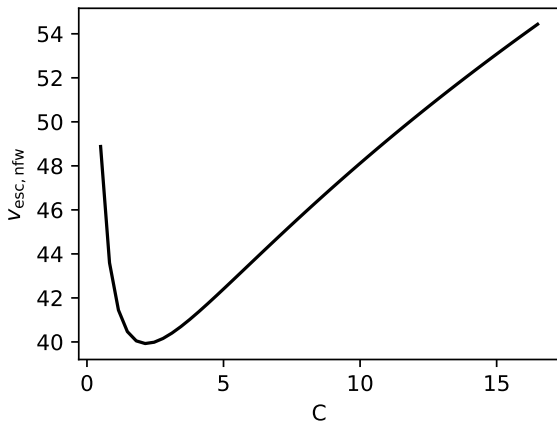


Figure 6. Central escape velocity depending on the concentration of NFW profile. M_{vir} and r_{vir} are chosen from the NFWstd halo.

final masses can be above $100 M_{\odot}$, larger than most detected GW events from LVK (The LIGO Scientific Collaboration et al. 2021).

We did not find IMBH formation for $W_0 = 6$ even during the long-term evolution. An IMBH may form via hierarchical mergers of BHs, like the extremely dense GC (Giersz et al. 2015) and galactic center (Antonini et al. 2019; Kroupa et al. 2020). However, the density in the Pop3 model is not sufficient to trigger on this channel.

Figure 9 shows the average values and the standard derivations of n_{merge} , $m_{f,max}$, and the mass ratios (q) of BBH mergers (including

IMBHs) for the long-term models. As observed, a higher density of dark matter halo results in a larger average n_{merge} and a larger average $m_{f,max}$. This is expected as the collision rate is higher for denser clusters under a denser dark matter halo. Our models without dark matter halo can also generate IMBH-BH mergers. But this is unlikely to occur in the real galactic environment, as these star clusters easily suffer tidal disruption.

3.4 Mergers in pair-instability mass gap

We also counted the mergers with PIBHs, which should originate from binary stellar evolution or BBH mergers. Table 4 shows the average number of mergers including PIBHs. The models with $W_0 = 6$ have a systematically higher number of mergers with PIBHs compared to that of the models with $W_0 = 9$. Thus, IMBHs can suppress the formation of PIBHs. There are two possible reasons: the formation of VMSs can reduce the number of massive-star binaries that can form PIBHs; and the existence of IMBHs suppresses the formation of low-mass binaries with PIBHs. Among all merger types, PIBH-LBH contributes the most.

The presence of mergers with PIBHs is a striking feature of BH mergers in Pop3 star clusters. Isolated Pop3 binary stars cannot form such BH mergers (Hijikawa et al. 2021), unless we assume inefficient convective overshoot in Pop3 single star evolution (Tanikawa et al. 2021a), or detail modeling of mass transfer in Pop3 binary stars (Kinugawa et al. 2021). Liu & Bromm (2020) shows that Pop3 star clusters can form PIBH-LBH like GW190521 (Abbott et al. 2020a). In contrast, Table 4 clearly shows that Pop3 star clusters can be

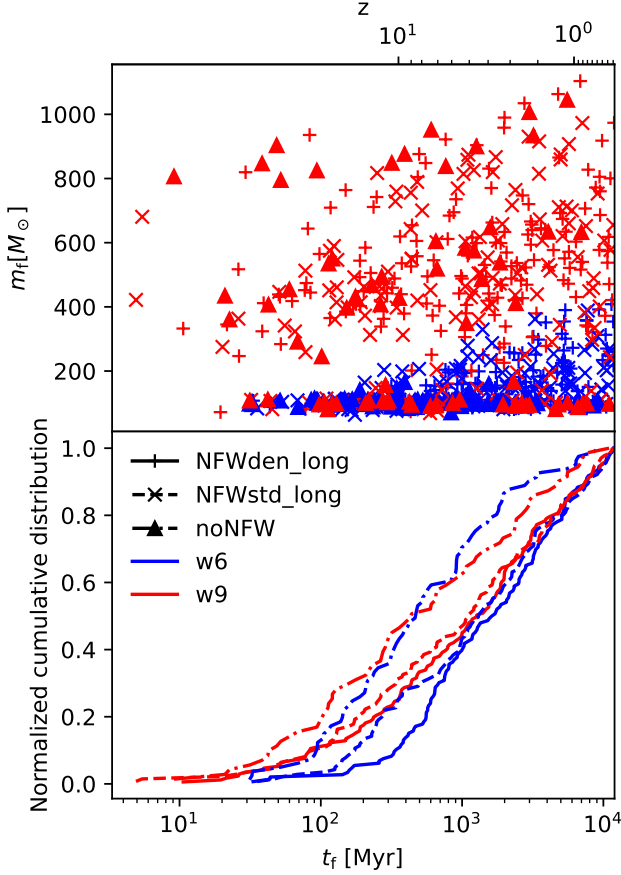


Figure 7. Upper panel: m_f of each merger of two BHs or IMBHs for all long-term models. Lower panel: the normalized cumulative distribution of the merger time (t_f). The corresponding redshift (z) is shown in the upper x-axis.

Table 4. Average number of mergers including pair instability mass gap BH (PIBH) for the long-term models. BPIBH indicates that both binary members are PIBHs; LBH is low-mass BH ($< 60 M_\odot$).

Halo	King	IMBH-PIBH	BPIBH	PIBH-LBH
NFWden	w6	0.12	0.094	0.88
NFWden	w9	0.062	0	0.094
NFWstd	w6	0.062	0.031	0.88
NFWstd	w9	0.031	0	0.16
noNFW	w6	0	0	0.22
noNFW	w9	0	0	0.062

formation sites of a wide variety of mergers with PIBHs including IMBH-PIBHs and BPIBHs, independently of Pop3 single and binary star evolution.

GW190521 is considered to contain at least one PIBH (Abbott et al. 2020a), although it can be an IMBH-LBH merger (Fishbach & Holz 2020; Nitz & Capano 2021). From Figure 8, various mass combinations of BH mergers with the total mass of approximately $150 M_\odot$ can be observed. If we regard PIBH-LBH mergers as GW190521-like mergers, the PIBH-LBH merger rate is $0.01 - 0.15 \text{ yr}^{-1} \text{ Gpc}^{-3}$, which is comparable to the inferred merger rate of GW190521-like mergers (Abbott et al. 2020b). Thus, Pop3 star clusters could repro-

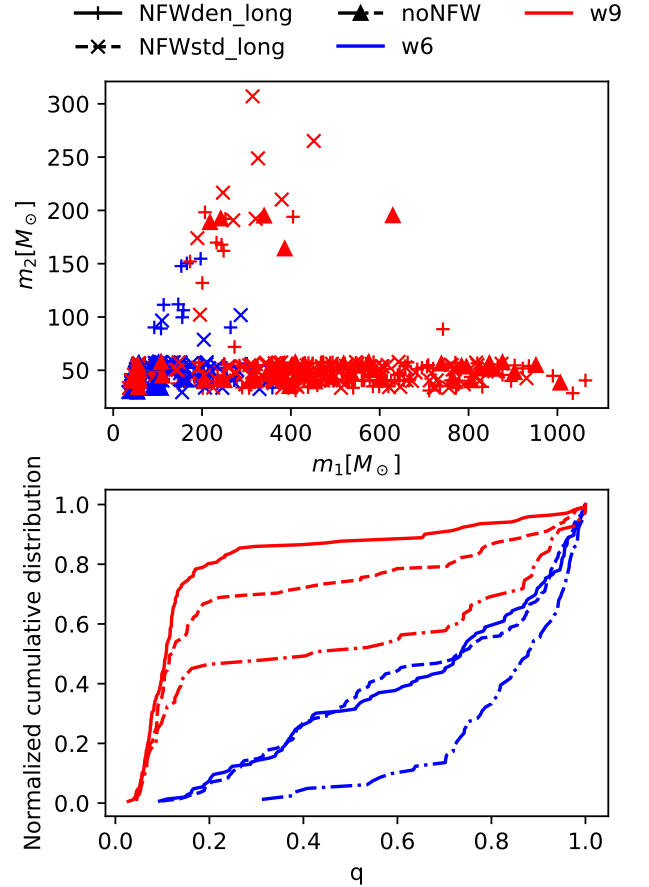


Figure 8. Upper panel: m_1 v.s. m_2 of each merger of two BHs or IMBHs for all long-term models. Lower panel: normalized cumulative distribution of the mass ratio (q).

duce GW190521. Here, we have to remark that GW190521 can be formed not only in Pop3 star clusters, but also in isolated binary stars (Belczynski 2020; Kinugawa et al. 2021; Tanikawa et al. 2021a), young star clusters (Di Carlo et al. 2020; Kremer et al. 2020; Arca-Sedda et al. 2021; González et al. 2021; Rizzuto et al. 2021), globular clusters (Rodríguez et al. 2019), and galactic centers (Tagawa et al. 2021; Fragione et al. 2022a).

3.5 Peak frequency and characteristic strain for GW detection

The IMBH-BH and BBH mergers in the Pop3 star clusters can be detected by the future space-borne GW detectors, like LISA, TianQin, and Taiji. We calculated the peak frequency (f_{peak}) of GW detection and characteristic strain of our mergers. We adopted the estimation of f_{peak} from Hamers (2021), which is an improved version for low eccentric binaries based on Wen (2003). The detail formula is:

$$f_{\text{peak}} = \frac{\sqrt{G(m_1 + m_2)}}{\pi} \frac{1 - 1.01678e + 5.57372e^2 - 4.9271e^3 + 1.68506e^4}{[a(1 - e^2)]^{1.5}} \quad (15)$$

The upper panel of Figure 10 shows $1 - e$ v.s. f_{peak} . The evolution curves are integrated using \dot{a} and \dot{e} based on the secular change

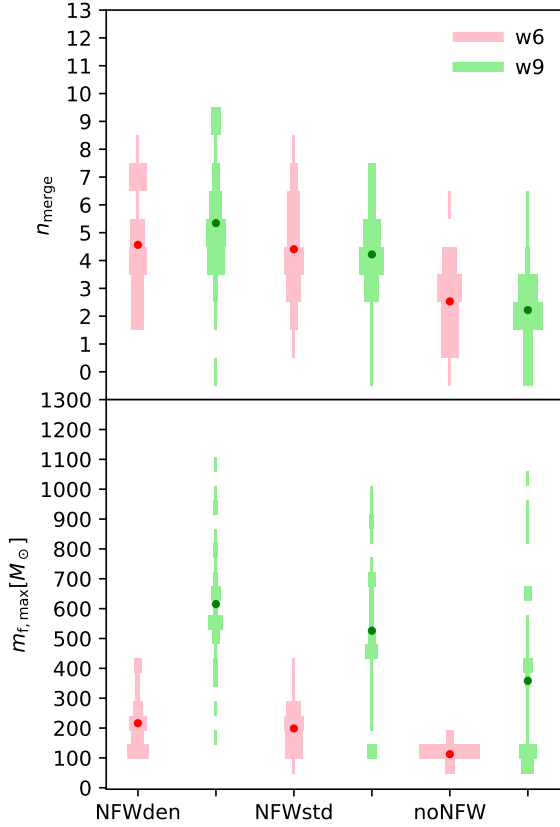


Figure 9. Average number of mergers and the final maximum masses of BHs for the long-term models. The plotting style is similar to that of Figure 2.

estimation from Peters (1964):

$$\begin{aligned} \dot{a} &= -\frac{\beta F(e)}{a^3}, \\ \dot{e} &= -\frac{19}{12} \frac{\beta e}{a^4 (1-e^2)^{5/2}} \left(1 + \frac{121}{304} e^2\right), \end{aligned} \quad (16)$$

where the factor,

$$\begin{aligned} F(e) &= \sum_{n=1}^{\infty} g(n, e) \\ &= \frac{1}{(1-e^2)^{7/2}} \left(1 + \frac{73}{24} e^2 + \frac{37}{96} e^4\right), \\ \beta &= \frac{64}{5} \frac{G^3 m_1 m_2 (m_1 + m_2)}{c^5}. \end{aligned} \quad (17)$$

Here, $g(n, e)$ is Equation 20 from Peters & Mathews (1963), and c is the speed of light. The integration stops when e approaches zero.

We calculated the characteristic strain ($h_{c,n}$) corresponding to f_{peak} by using the formula from Kremer et al. (2019):

$$h_{c,n}^2 = \frac{2}{3\pi^{4/3}} \frac{G^{5/3} M_{c,z}^{5/3}}{c^3 D^2} \frac{1}{f_{n,z}^{1/3} (1+z)^2} \frac{2^{2/3} g(n, e)}{n F(e)}, \quad (18)$$

where $M_{c,z}$ is the observed chirp mass with the redshift z , and $f_{n,z}$ is the observed frequency of the n th harmonic. n can be calculated by $f_{\text{peak}}/f_{\text{orb}}$, where f_{orb} is the rest-frame frequency of a binary. With the limited observation time, T_{obs} , $h_{c,n}$ is multiplied by the square root of $\min[1, \dot{f}_n(T_{\text{obs}}/f_n)]$ where f_n is the rest-frame frequency

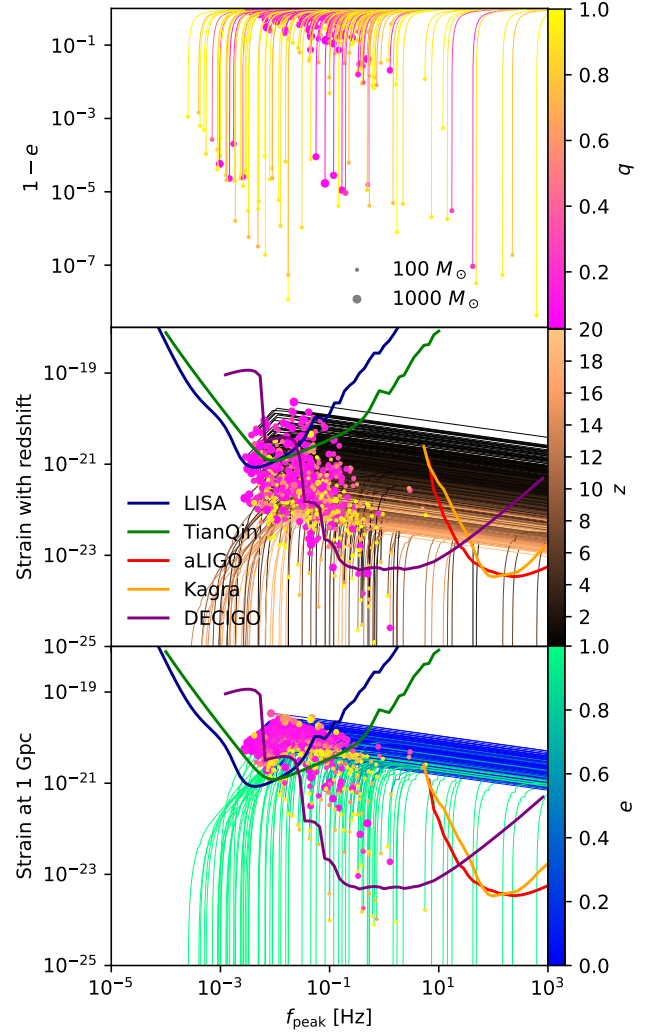


Figure 10. Eccentricity, peak frequency of GW signals (f_{peak}) and, characteristic strain of all IMBH-BH and BBH mergers in the long-term models. Symbols show the initial condition of each binary and curves show their evolution due to the GW radiation. Sizes of symbols indicate the total masses of binaries; colors indicate the mass ratios (q) for the upper panel, redshift (z) for the central panel, and e (curve colors) for the lower panel. z with corresponding Hubble distance is used to evaluate strain for the central panel, whereas a fixed distance of 1 Gpc with $z \approx 0.233$ is assumed for the strain in the lower panel. The sensitivity curves of 5 GW detectors are shown.

with n th harmonic ($f_n = f_{\text{peak}}$ in our calculation). We adopted that $T_{\text{obs}} = 4$ years.

We found a group of extremely eccentric IMBH-BH and BBH mergers with $1 - e < 10^{-5}$. Some even have $1 - e < 10^{-7}$. Their f_{peak} spreads in a large region.

The central panel of Figure 10 shows the characteristic strain of each merger vs. f_{peak} considering z and the corresponding Hubble distances. Their z are estimated by t_f as shown in Figure 7. The hubble distances are calculated by $c z / H_0$. We also plot the space-borne GW detectors, LISA, TianQin and DECIGO, sensitivity curves (Robson et al. 2019; Wang et al. 2019; Kawamura et al. 2011), and the ground-based detectors, advanced LIGO (aLIGO) and Kagra (Miller et al. 2015; Michimura et al. 2020). The Taiji mission has a similar planned arm length to that of LISA; thus, we expect its sensitivity

curve to be close to that of LISA. For LISA, TianQin, and Taiji, a part of low- z mergers can be detected. Most mergers can be covered by DECIGO, aLIGO, and Kagra. In simulations, the initial a and e of mergers are not recorded at the times when the binaries form, but at the times slightly earlier than t_f (depending on the integration time step sizes). Thus, the starting points of some mergers are already inside the detectable region.

The lower panel of Figure 10 shows the strain of mergers assuming all events occur at 1 Gpc with $z \approx 0.233$, ignoring their merger times. In this case, most mergers including all range of eccentricities can be covered by all detectors.

3.6 Estimation of IMBH-BH merger rate

To estimate the IMBH-BH merger rate based on our models, the total stellar mass of Pop3 star clusters in the past must be obtained. Tanikawa et al. (2022) provided a fitting formula (Equation 5) to the Pop3 star formation rate density from Skinner & Wise (2020). The integration of the formula from 100 to 500 Myr (redshift from 20 to 10) indicates that the total stellar mass is approximately $3.2 \times 10^4 M_\odot \text{Mpc}^{-3}$. This estimation is an average value based on the numerical models of Skinner & Wise (2020). Inayoshi et al. (2021) suggested that the upper limit of Pop3 star formation rate inferred by re-ionization history is $2 \times 10^5 M_\odot \text{Mpc}^{-3}$. Assuming the average n_{merge} is 5 per 12 Gyr as shown in Figure 9 for NFWden, the expected upper limit of IMBH-BH merger rate is $0.1 - 0.8 \text{ yr}^{-1} \text{Gpc}^{-3}$ depending on the two star formation rate. It is slightly larger than the estimated merger rate of $< 0.01 \text{ yr}^{-1} \text{Gpc}^{-3}$ from Tanikawa et al. (2021b), and comparable to the upper limit from The LIGO Scientific Collaboration et al. (2021). Considering the redshift dependence of the merger rate shown in Figure 7, the chance to detect GW events from the Pop3 star clusters at $z > 6$ is expected to be considerably higher than the average rate.

3.7 IMBH-star mergers

Generally, most of IMBHs in all types of environments grow their masses through IMBH-BH mergers. In contrast, part of them grow through mergers with main-sequence (MS), post main-sequence, and HeMS. Such mergers can trigger tidal disruption events launching relativistic jets (Kashiyama & Inayoshi 2016). We discuss about their detectability later in this section.

In the Pop3 star clusters with a top-heavy IMF, BHs are the major members of the cluster during the long-term evolution. They occupy the center of the cluster. Thus, IMBH-star mergers during the long-term evolution are unlikely to be formed, but they can occur at the early phase (within 10 Myr after the birth of stars). We detected IMBH-star mergers in all short-term and long-term models, by selecting the mergers where $m_{\text{imbh}} > m_{\text{star}}$. For mergers with $m_{\text{imbh}} < m_{\text{star}}$, we counted them as IMBH-VMS mergers in Table 3. There is no IMBH-VMS in the long-term models.

Figure 11 show the properties of IMBH-star mergers. Most of mergers occur between 2.0 to 2.5 Myr. The secondary stars can be MSs, core Helium burning stars (CHeBs), FAGBs, and HeMSs, where the last two are major ones. The masses of FAGBs and of most HeMSs range from $60 - 180 M_\odot$ and $60 - 100 M_\odot$, respectively. The primary IMBHs have masses below $400 M_\odot$, except two mergers of IMBH-MS and IMBH-FAGB. Most IMBH-FAGB mergers have a ranging from $100 - 3000 R_\odot$ and circular orbits, whereas most IMBH-HeMS mergers have smaller a ranging from $10 - 600 R_\odot$ and nearly circular orbits. A few high-eccentric orbits also exist. Particularly,

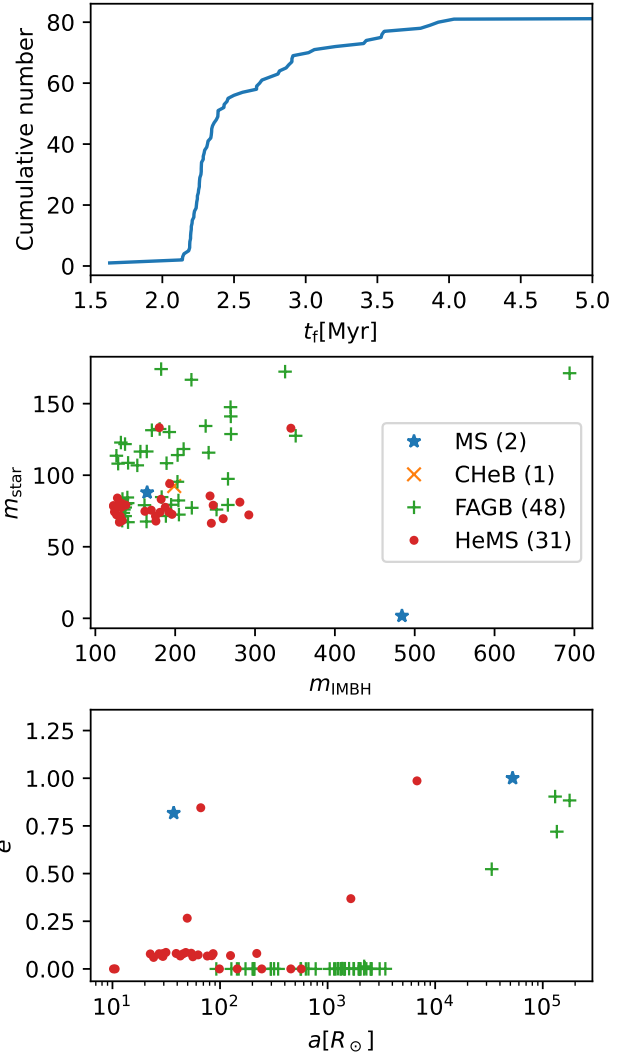


Figure 11. Properties of IMBH-star mergers. The upper panel: the cumulative distribution of t_f . The middle panel: Masses of stars (m_{star}) v.s. masses of IMBHs (m_{imbh}). The lower panel: a v.s. e . The meaning of symbols: MS: main sequence; CHeB: core Helium burning; FAGB: first asymptotic giant; HeMS: main-sequence naked Helium star.

the two IMBH-MS mergers have $e > 0.75$. In the bSE treatment, all IMBH-FAGB and IMBH-HeMS mergers are Thorne-Zytkow objects that IMBHs do not accrete material from companions.

Kashiyama & Inayoshi (2016) suggested that prompt emission of relativistic jets launched by tidal disruption events will be observed in soft X-ray bands $\lesssim 10 \text{ keV}$ because of the high-redshift nature of Pop3 star clusters. They found that the peak isotropic luminosity of prompt emission is:

$$L_{\text{xray}} \sim 8 \times 10^{50} \text{ erg s}^{-1} \left(\frac{m_{\text{IMBH}}}{10^5 M_\odot} \right)^{-1/2} \left(\frac{m_{\text{star}}}{40 M_\odot} \right)^2 \left(\frac{R_{\text{star}}}{3 R_\odot} \right)^{-3/2}, \quad (19)$$

where they suppose that BHs are formed from supermassive stars with $\sim 10^5 M_\odot$, and Pop3 MSs are disrupted. Figure 11 shows that $60 - 150 M_\odot$ FAGBs and $60 - 100 M_\odot$ HeMSs are disrupted by BHs with $100 - 300 M_\odot$ in our Pop3 star clusters. The peak luminosity is

$\sim 10^{48}$ erg s^{-1} in the FAGB case, as their stellar radii are $\sim 3000R_{\odot}$. In contrast, the peak luminosity can reach $\sim 10^{52}$ erg s^{-1} in the HeMS case because of their compactness. As the observed flux in the HeMS case is larger than 10^{-9} erg s^{-1} cm^{-2} even at a redshift of 20, tidal disruption events of HeMSs in Pop3 star clusters can be discovered by eROSITA with a limiting flux of $\sim 10^{-12}$ erg s^{-1} cm^{-2} (Merloni et al. 2012).

4 DISCUSSION

The estimated merger rate is high as discussed in Section 3.6. However, our N -body models only cover a small parameter space of Pop3 star clusters. We discuss how the formation of VMS and the merger rate depend on a few uncertain factors

Firstly, the NFW profile is a simply approximation of real mini dark matter halos, which can grow up via mergers or can be disrupted by the tide from a massive host environment. During a merger, two embedded star clusters may also merge. Such an impact is difficult to estimate unless a self-consistent hydrodynamic model like that in Sakurai et al. (2017) is performed for 12 Gyr, which is particularly challenging due to the time-consuming computing. The NFWden and the NFWstd dark matter halos have a density difference of approximately 8 times, whereas the n_{merge} only differ by one. The influence is not significant. If the halo grows up, the star cluster may be denser and generate more mergers. If the halo is tidally disrupted or absorbed by the massive host environment, the star cluster might also dissolve. It is still possible that the final remnant of the system is an IMBH-BH binary that can merge today.

The formation of VMS is determined by the collision timescale described by Equation 11, which depends on the initial central density of Pop3 star clusters. For $W_0 = 6$ of King model, the formation of VMS does not occur, and no IMBH forms. This density profile is close to the Plummer model, which is commonly used to describe the morphology of star clusters after dynamical virialization and before core collapse. During the cluster formation stage, the morphology of the cluster is highly irregular with a high central density, as shown in the hydrodynamical simulation from Sakurai et al. (2017). Thus, considering a more realistic condition, the chance to form a VMS in Pop3 star cluster is higher.

We assume that all Pop3 stars form in the star clusters with $M_{\text{sc}} = 10^5 M_{\odot}$. This is probably not the case, a more realistic assumption is that the total mass of Pop3 star clusters follow a distribution peaking around $10^5 M_{\odot}$. For low-mass clusters, if the central density is sufficiently high ($\rho_{10} > 7 \times 10^5 M_{\odot} \text{pc}^{-3}$), the multiple mergers of MS stars may occur and VMSs may form. Sakurai et al. (2017) show that all Pop3 star clusters with M_{sc} from 5×10^4 to $1.6 \times 10^5 M_{\odot}$ satisfy this criterion, and there is no clear correlation between core densities of clusters and M_{sc} . In their model, the lowest M_{sc} had the highest core density. Thus, we expect that the formation rate of VMSs in Pop3 star clusters with $M_{\text{sc}} \geq 1 \times 10^4 M_{\odot}$ to be high. A part of low-mass Pop3 clusters may not form VMSs. The threshold of M_{sc} is unclear. With a top-heavy IMF, few stars can form in a low-mass cluster. Thus, we expect that the threshold to be around $10^3 - 10^4 M_{\odot}$. Under the dark matter halo, all Pop3 star clusters can still survive and produce GW mergers. A low-mass gas cloud may form a single VMS instead of a low-mass star cluster. Then, an IMBH can form but no GW merger occurs. Thus, our estimation of merger rate is an upper limit, considering such uncertainty.

The assumption of top-heavy IMF based on the theoretical models of Pop3 star formation may be updated to more realistic models in the future. However, we expect that different IMFs weakly affect

the merger rate. The models of Sakurai et al. (2017) assumed the canonical IMF (Salpeter 1955; Kroupa 2001; Chabrier 2003), and also produced IMBH seeds. Mergers may occur with a top-heavy IMF, but the merger rate per BH would be lower compared to that of a canonical IMF because of a lower central density caused by the initial strong stellar winds from massive stars and the binary heating (Wang et al. 2021).

The upper mass limit of IMF is $150 M_{\odot}$ in our models, which was commonly assumed for Population I and II stars (Kroupa 2001). For Pop3 stars, the upper mass can be considerably higher, even reaching $1000 M_{\odot}$ if only a single star is allowed to form in a halo (Hirano et al. 2015; Hosokawa et al. 2016). If the maximum mass is higher, the formation of IMBH becomes easier.

There is no primordial binary in our models. Observations of the young star-forming region show that OB stars are mostly in multiple systems (Sana et al. 2012). It is unclear whether the formation of Pop3 stars follows the same tendency. However, with primordial binaries, we expect that the mergers rate to be higher and the formation of VMSs to become easier. As shown in Wang et al. (2022), the structure (density profile) evolution of star clusters weakly depends on the fraction of primordial binaries of OB stars. With OB stars all in binaries initially, the dynamically driven mergers of BBHs increases. Thus, we expect IMBH-BH mergers during the long-term evolution to also increase.

In our simulations, the mergers of BBHs are treated by the BSEEMP code using the orbital shrinking from Peters (1964). The GW kick is not considered. When IMBH-BH merges, the high-velocity kick due to anisotropy of GW emission can eject the merger from the cluster. The kick velocity depends on q and the spins of BHs. The mean kick velocity roughly linearly increases from 0 to 200 pc Myr^{-1} in the range of q from 0 to 0.2, as shown in Morawski et al. (2018), which is based on the formula from Baker et al. (2008). v_{esc} is 50–70 pc Myr^{-1} for our models with dark matter halos, as discussed in Section 3.2. Thus, if the IMBH mass is not sufficiently large, an IMBH-BH merger may eject the IMBH from the cluster. This can reduce the IMBH-BH merger rate, whereas the BBH merger rate may not be considerably influenced. If the dark matter halo is much denser than the NFWden halo, where $v_{\text{esc}} > 200$ pc Myr^{-1} , we expect that IMBHs can also be trapped and the merger rate is consistent with our model. The initial masses of IMBHs are not affected by the GW kick as they form via the stellar evolution of massive main sequence stars.

5 CONCLUSIONS

In this work, we conducted a series of N -body simulations for Pop3 star clusters embedded in static mini dark matter halos. We investigated how VMSs and IMBHs form depending on the initial conditions of star clusters. We found that the dark matter halos can trap the Pop3 star clusters such that they can survive until today and continue to produce BBH and IMBH-BH mergers. The low- z mergers can be detected by the space-borne GW detectors, including LISA, TianQin, and Taiji, and most mergers can be detected by DECIGO, aLIGO, and Kagra. The merger rate is high; thus, the GW events from Pop3 star clusters can be an important contribution to the future GW detection.

We found that the central density is the major parameter that determines whether multiple mergers can occur in a short time (≤ 2 Myr) to form a VMS. The dynamically formed binaries via three-body channel are the major sources for the mergers. For King model with $W_0 = 9$ and 12, the collision rate is sufficiently high (Equation 11)

to drive multiple mergers within a short time to form a VMS before the stellar wind removes most of the mass (Figure 3). For $W_0 = 6$, the multiple mergers do not occur; thus, no VMS forms. However, the high central density that can form a VMS as shown in Sakurai et al. (2017) is a more realistic condition at the early phase. Other parameters, including the degree of primordial mass segregation, the lower mass boundary of IMF, and properties of dark matter halos, have almost no influence on the formation of VMS.

The extremely metal-poor VMS eventually evolves to an IMBH with mass above $400 M_\odot$ via three possible modes: single stellar evolution, binary stellar evolution, and mass accretion in a BH-VMS system (Figures 2 and 4). With a dark matter halo, the Pop3 star cluster can keep r_h below 10 pc for 12 Gyr (Figure 5) because it significantly increases v_{esc} of stars and suppresses the tidal evaporation of star clusters. Thus, if the dark matter halo still survives today, a dark cluster might exist at the center and can produce BBH and IMBH-BH mergers, that might be observed by the GW detector. Without dark matter halo, the cluster expands quickly in approximately 1 Gyr, the galactic tide can easily disrupt the cluster, similar to the fate of young star clusters with few thousands stars. In this case, the cluster might leave an IMBH-BH system eventually.

The estimation of the characteristic strain and f_{peak} indicates that a part of IMBH-BH and BBH mergers with low- z in our models are above the sensitivity limit of LISA, TianQin and Taiji, and most mergers are covered by DECIGO, aLIGO and Karga in the high-frequency region (Figure 10). If we assume that mergers occur within 1 Gpc ($z \approx 0.233$), most events can be covered by all detectors. We also found that the extremely high-eccentric mergers can form in Pop3 star clusters, where $1 - e$ can reach 10^{-8} . They cannot be detected by LISA, TianQin, and Taiji, but can be interesting sources for other detectors. Mergers with PIBHs can also occur. The PIBHs can form via weak wind from extremely metal-poor stars, binary stellar evolution, and BBH mergers.

There are also mergers of IMBH-star binaries, where the stars can be MS, CHeB, FAGB, or HeMS, where the latter two are the major contributors. They can evolve to Thorne-Zytkow objects where IMBHs do not accrete material during the merging process. The tidal disruption events of HeMSs can be discovered by eROSITA with a limiting flux of $\sim 10^{-12} \text{ erg s}^{-1} \text{ cm}^{-2}$.

Based on the star formation rate of Pop3 stars from Skinner & Wise (2020) and Inayoshi et al. (2021), we estimate the upper limit of IMBH-BH merger rate is approximately $0.1 - 0.8 \text{ yr}^{-1} \text{ Gpc}^{-3}$. The mergers can occur at any z from 20 to 0, whereas a large fraction (0.4–0.8) occurs between 6 to 20 (Figure 7). The PIBH-LBH merger rate is $0.01 - 0.15 \text{ yr}^{-1} \text{ Gpc}^{-3}$, which is comparable to the merger rate from other channels. Thus, the GW190521-like mergers are also possible from Pop3 star clusters.

Considering the GW kick, a part of IMBHs might be ejected after GW mergers, which might reduce the total merger rate. The disruption of dark matter halo can also reduce the merger rate. If many Pop3 stars are in low-mass star clusters where $M_{\text{sc}} \ll 10^4 M_\odot$, the total number of IMBHs can also be lower. Even considering this effect, the IMBH-BH mergers from Pop3 star clusters can still be an important contribution to the GW events that can be detected by the new generation of GW detectors.

ACKNOWLEDGEMENTS

L.W. thanks the support from the one-hundred-talent project of Sun Yat-sen University, the Fundamental Research Funds for the Central Universities, Sun Yat-sen University (22hytd09) and the National

Natural Science Foundation of China through grant 12073090. L.W. also thanks the financial support from JSPS International Research Fellow (Graduate School of Science, The University of Tokyo). This work is partly supported from the Grants-in-Aid for Scientific Research (17H06360, 19K03907). We thank Yi-Ming Hu for providing the data of sensitivity curve of TianQin.

DATA AVAILABILITY

The simulations underlying this article were performed on the personal computing server of the first author. The data were generated by the software `PETAR`, which is available in GitHub, at <https://github.com/lwang-astro/PeTar>. The stellar evolution code `BSEEMP` is also available in GitHub <https://github.com/atrnkw/bseemp>. The initial conditions of star cluster models are generated by the software `MCLUSTER` (Küpper et al. 2011), which is available in GitHub, at <https://github.com/lwang-astro/mcluster>. The simulation data will be shared via private communication with a reasonable request.

REFERENCES

- Abbott B. P., et al., 2019, *Phys. Rev. D*, **100**, 064064
 Abbott R., et al., 2020a, *Phys. Rev. Lett.*, **125**, 101102
 Abbott R., et al., 2020b, *ApJ*, **900**, L13
 Abbott R., et al., 2021, *Physical Review X*, **11**, 021053
 Amaro-Seoane P., et al., 2022, arXiv e-prints, p. arXiv:2203.06016
 Anderson J., van der Marel R. P., 2010a, *ApJ*, **710**, 1032
 Anderson J., van der Marel R. P., 2010b, *ApJ*, **710**, 1032
 Antonini F., Gieles M., Gualandris A., 2019, *MNRAS*, **486**, 5008
 Arca-Sedda M., Rizzuto F. P., Naab T., Ostriker J., Giersz M., Spurzem R., 2021, *ApJ*, **920**, 128
 Baker J. G., Boggs W. D., Centrella J., Kelly B. J., McWilliams S. T., Miller M. C., van Meter J. R., 2008, *ApJ*, **682**, L29
 Banerjee S., Kroupa P., 2011, *ApJ*, **741**, L12
 Banerjee S., Belczynski K., Fryer C. L., Berczik P., Hurley J. R., Spurzem R., Wang L., 2020, *A&A*, **639**, A41
 Barth A. J., Ho L. C., Rutledge R. E., Sargent W. L. W., 2004, *ApJ*, **607**, 90
 Baumgardt H., 2017, *MNRAS*, **464**, 2174
 Baumgardt H., Hut P., Makino J., McMillan S., Portegies Zwart S., 2003a, *ApJ*, **582**, L21
 Baumgardt H., Makino J., Hut P., McMillan S., Portegies Zwart S., 2003b, *ApJ*, **589**, L25
 Baumgardt H., et al., 2019, *MNRAS*, **488**, 5340
 Belczynski K., 2020, *ApJ*, **905**, L15
 Belczynski K., et al., 2016, *A&A*, **594**, A97
 Binney J., Tremaine S., 1987, Galactic dynamics
 Bovy J., 2015, *ApJS*, **216**, 29
 Bryan G. L., Norman M. L., 1998, *ApJ*, **495**, 80
 Chabrier G., 2003, *PASP*, **115**, 763
 Chilingarian I. V., Katkov I. Y., Zolotukhin I. Y., Grishin K. A., Beletsky Y., Boutsia K., Osip D. J., 2018, *ApJ*, **863**, 1
 Chon S., Omukai K., Schneider R., 2021, *MNRAS*, **508**, 4175
 Cropper M., Soria R., Mushotzky R. F., Wu K., Markwardt C. B., Pakull M., 2004, *MNRAS*, **349**, 39
 Davis S. W., Narayan R., Zhu Y., Barret D., Farrell S. A., Godet O., Servillat M., Webb N. A., 2011, *ApJ*, **734**, 111
 Di Carlo U. N., Mapelli M., Bouffanais Y., Giacobbo N., Santoliquido F., Bressan A., Spera M., Haardt F., 2020, *MNRAS*, **497**, 1043
 Event Horizon Telescope Collaboration et al., 2019, *ApJ*, **875**, L1
 Fan H.-M., Hu Y.-M., Barausse E., Sesana A., Zhang J.-d., Zhang X., Zi T.-G., Mei J., 2020, *Phys. Rev. D*, **102**, 063016
 Farrell S. A., Webb N. A., Barret D., Godet O., Rodrigues J. M., 2009, *Nature*, **460**, 73

- Farrell S. A., et al., 2012, *ApJ*, **747**, L13
- Feldmeier A., et al., 2013, *A&A*, **554**, A63
- Fishbach M., Holz D. E., 2020, *ApJ*, **904**, L26
- Fragione G., Bromberg O., 2019, *MNRAS*, **488**, 4370
- Fragione G., Silk J., 2020, *MNRAS*, **498**, 4591
- Fragione G., Loeb A., Kocsis B., Rasio F. A., 2022a, arXiv e-prints, p. [arXiv:2204.03745](https://arxiv.org/abs/2204.03745)
- Fragione G., Kocsis B., Rasio F. A., Silk J., 2022b, *ApJ*, **927**, 231
- Freitag M., Gürkan M. A., Rasio F. A., 2006, *MNRAS*, **368**, 141
- Fryer C. L., Belczynski K., Wiktorowicz G., Dominik M., Kalogera V., Holz D. E., 2012, *ApJ*, **749**, 91
- Gebhardt K., Rich R. M., Ho L. C., 2002, *ApJ*, **578**, L41
- Gebhardt K., Rich R. M., Ho L. C., 2005, *ApJ*, **634**, 1093
- Gerssen J., van der Marel R. P., Gebhardt K., Guhathakurta P., Peterson R. C., Pryor C., 2002, *AJ*, **124**, 3270
- Gerssen J., van der Marel R. P., Gebhardt K., Guhathakurta P., Peterson R. C., Pryor C., 2003, *AJ*, **125**, 376
- Ghez A. M., Klein B. L., Morris M., Becklin E. E., 1998, *ApJ*, **509**, 678
- Ghez A. M., Salim S., Hornstein S. D., Tanner A., Lu J. R., Morris M., Becklin E. E., Duchêne G., 2005, *ApJ*, **620**, 744
- Ghez A. M., et al., 2008, *ApJ*, **689**, 1044
- Giersz M., Leigh N., Hypki A., Lützgendorf N., Askar A., 2015, *MNRAS*, **454**, 3150
- Gillessen S., Eisenhauer F., Trippe S., Alexander T., Genzel R., Martins F., Ott T., 2009, *ApJ*, **692**, 1075
- Gillessen S., et al., 2017, *ApJ*, **837**, 30
- Gómez F. A., Helmi A., Brown A. G. A., Li Y.-S., 2010, *MNRAS*, **408**, 935
- González E., Kremer K., Chatterjee S., Fragione G., Rodríguez C. L., Weatherford N. C., Ye C. S., Rasio F. A., 2021, *ApJ*, **908**, L29
- Greene J. E., Ho L. C., 2004, *ApJ*, **610**, 722
- Greene J. E., Strader J., Ho L. C., 2020, *ARA&A*, **58**, 257
- Gültekin K., Miller M. C., Hamilton D. P., 2004, *ApJ*, **616**, 221
- Hamers A. S., 2021, *Research Notes of the American Astronomical Society*, **5**, 275
- Heger A., Fryer C. L., Woosley S. E., Langer N., Hartmann D. H., 2003, *ApJ*, **591**, 288
- Hijikawa K., Tanikawa A., Kinugawa T., Yoshida T., Umeda H., 2021, *MNRAS*, **505**, L69
- Hills J. G., Day C. A., 1976, *Astrophys. Lett.*, **17**, 87
- Hirano S., Hosokawa T., Yoshida N., Omukai K., Yorke H. W., 2015, *MNRAS*, **448**, 568
- Hopman C., Portegies Zwart S. F., Alexander T., 2004, *ApJ*, **604**, L101
- Hosokawa T., Hirano S., Kuiper R., Yorke H. W., Omukai K., Yoshida N., 2016, *ApJ*, **824**, 119
- Hurley J. R., 2007, *MNRAS*, **379**, 93
- Hurley J. R., Pols O. R., Tout C. A., 2000, *MNRAS*, **315**, 543
- Hurley J. R., Tout C. A., Pols O. R., 2002, *MNRAS*, **329**, 897
- Inayoshi K., Kashiyama K., Visbal E., Haiman Z., 2021, *ApJ*, **919**, 41
- Ishiyama T., et al., 2021, *MNRAS*, **506**, 4210
- Iwasawa M., Tanikawa A., Hosono N., Nitadori K., Muranushi T., Makino J., 2016, *PASJ*, **68**, 54
- Iwasawa M., Namekata D., Nitadori K., Nomura K., Wang L., Tsubouchi M., Makino J., 2020, *PASJ*, **72**, 13
- Jani K., Shoemaker D., Cutler C., 2020, *Nature Astronomy*, **4**, 260
- Kaaret P., Prestwich A. H., Zezas A., Murray S. S., Kim D. W., Kilgard R. E., Schlegel E. M., Ward M. J., 2001, *MNRAS*, **321**, L29
- Kamizasa N., Terashima Y., Awaki H., 2012, *ApJ*, **751**, 39
- Kashiyama K., Inayoshi K., 2016, *ApJ*, **826**, 80
- Kawamura S., et al., 2011, *Classical and Quantum Gravity*, **28**, 094011
- King I. R., 1966, *AJ*, **71**, 64
- Kinugawa T., Nakamura T., Nakano H., 2021, *MNRAS*, **501**, L49
- Kızıltan B., Baumgardt H., Loeb A., 2017, *Nature*, **542**, 203
- Kong A. K. H., Di Stefano R., Yuan F., 2004, *ApJ*, **617**, L49
- Körding E., Falcke H., Markoff S., 2002, *A&A*, **382**, L13
- Kormendy J., Ho L. C., 2013, *ARA&A*, **51**, 511
- Kremer K., et al., 2019, *Phys. Rev. D*, **99**, 063003
- Kremer K., et al., 2020, *ApJ*, **903**, 45
- Kroupa P., 2001, *MNRAS*, **322**, 231
- Kroupa P., Subr L., Jerabkova T., Wang L., 2020, *MNRAS*, **498**, 5652
- Küpper A. H. W., Maschberger T., Kroupa P., Baumgardt H., 2011, *MNRAS*, **417**, 2300
- Lai K.-H., Hannuksela O. A., Herrera-Martín A., Diego J. M., Broadhurst T., Li T. G. F., 2018, *Phys. Rev. D*, **98**, 083005
- Lanzoni B., et al., 2013, *ApJ*, **769**, 107
- Lasota J. P., Alexander T., Dubus G., Barret D., Farrell S. A., Gehrels N., Godet O., Webb N. A., 2011, *ApJ*, **735**, 89
- Latif M. A., Whalen D., Khochfar S., 2022, *ApJ*, **925**, 28
- Leigh N. W. C., Lützgendorf N., Geller A. M., Maccarone T. J., Heinke C., Sesana A., 2014, *MNRAS*, **444**, 29
- Lin D., et al., 2018, *Nature Astronomy*, **2**, 656
- Liu B., Bromm V., 2020, *ApJ*, **903**, L40
- Liu S., Hu Y.-M., Zhang J.-d., Mei J., 2020, *Phys. Rev. D*, **101**, 103027
- Liu B., Meynet G., Bromm V., 2021, *MNRAS*, **501**, 643
- Luo J., et al., 2016, *Classical and Quantum Gravity*, **33**, 035010
- Lützgendorf N., Kissler-Patig M., Noyola E., Jalali B., de Zeeuw P. T., Gebhardt K., Baumgardt H., 2011, *A&A*, **533**, A36
- Lützgendorf N., Kissler-Patig M., Gebhardt K., Baumgardt H., Noyola E., Jalali B., de Zeeuw P. T., Neumayer N., 2012, *A&A*, **542**, A129
- Lützgendorf N., et al., 2013, *A&A*, **552**, A49
- Maccarone T. J., Servillat M., 2008, *MNRAS*, **389**, 379
- Mann C. R., et al., 2019, *ApJ*, **875**, 1
- Mapelli M., et al., 2021, *MNRAS*, **505**, 339
- Mapelli M., Bouffanais Y., Santoliquido F., Arca Sedda M., Artale M. C., 2022, *MNRAS*, **511**, 5797
- Matsumoto H., Tsuru T. G., Koyama K., Awaki H., Canizares C. R., Kawai N., Matsushita S., Kawabe R., 2001, *ApJ*, **547**, L25
- Mayer L., Kazantzidis S., Escala A., Callegari S., 2010, *Nature*, **466**, 1082
- Mayer L., Fiacconi D., Bonoli S., Quinn T., Roškar R., Shen S., Wadsley J., 2015, *ApJ*, **810**, 51
- McKernan B., Ford K. E. S., Lyra W., Perets H. B., 2012, *MNRAS*, **425**, 460
- McKernan B., Ford K. E. S., Kocsis B., Lyra W., Winter L. M., 2014, *MNRAS*, **441**, 900
- McNamara B. J., Harrison T. E., Anderson J., 2003, *ApJ*, **595**, 187
- Merloni A., et al., 2012, arXiv e-prints, p. [arXiv:1209.3114](https://arxiv.org/abs/1209.3114)
- Mezcua M., Roberts T. P., Lobanov A. P., Sutton A. D., 2015, *MNRAS*, **448**, 1893
- Mezcua M., Civano F., Marchesi S., Suh H., Fabbiano G., Volonteri M., 2018, *MNRAS*, **478**, 2576
- Michie R. W., 1963, *MNRAS*, **125**, 127
- Michimura Y., et al., 2020, *Phys. Rev. D*, **102**, 022008
- Miller M. C., Hamilton D. P., 2002, *MNRAS*, **330**, 232
- Miller J. M., Fabbiano G., Miller M. C., Fabian A. C., 2003, *ApJ*, **585**, L37
- Miller J., Barsotti L., Vitale S., Fritschel P., Evans M., Sigg D., 2015, *Phys. Rev. D*, **91**, 062005
- Morawski J., Giersz M., Askar A., Belczynski K., 2018, *MNRAS*, **481**, 2168
- Mouri H., Taniguchi Y., 2002, *ApJ*, **566**, L17
- Navarro J. F., Frenk C. S., White S. D. M., 1996, *ApJ*, **462**, 563
- Nitz A. H., Capano C. D., 2021, *ApJ*, **907**, L9
- Noyola E., Gebhardt K., Bergmann M., 2008, *ApJ*, **676**, 1008
- Oka T., Tsujimoto S., Iwata Y., Nomura M., Takekawa S., 2017, *Nature Astronomy*, **1**, 709
- Oshino S., Funato Y., Makino J., 2011, *PASJ*, **63**, 881
- Perera B. B. P., et al., 2017, *MNRAS*, **468**, 2114
- Peters P. C., 1964, *Physical Review*, **136**, 1224
- Peters P. C., Mathews J., 1963, *Physical Review*, **131**, 435
- Plummer H. C., 1911, *MNRAS*, **71**, 460
- Plunkett A. L., Fernández-López M., Arce H. G., Busquet G., Mardones D., Dunham M. M., 2018, *A&A*, **615**, A9
- Pooley D., Rappaport S., 2006, *ApJ*, **644**, L45
- Portegies Zwart S. F., McMillan S. L. W., 2002, *ApJ*, **576**, 899
- Portegies Zwart S. F., Baumgardt H., Hut P., Makino J., McMillan S. L. W., 2004, *Nature*, **428**, 724
- Portegies Zwart S. F., Baumgardt H., McMillan S. L. W., Makino J., Hut P., Ebisuzaki T., 2006, *ApJ*, **641**, 319
- Punturo M., et al., 2010, *Classical and Quantum Gravity*, **27**, 194002

Reinoso B., Schleicher D. R. G., Fellhauer M., Klessen R. S., Boekholt T. C. N., 2018, *A&A*, **614**, A14

Reitze D., et al., 2019, in *Bulletin of the American Astronomical Society*, p. 35 ([arXiv:1907.04833](https://arxiv.org/abs/1907.04833))

Rizzuto F. P., et al., 2021, *MNRAS*, **501**, 5257

Robson T., Cornish N. J., Liu C., 2019, *Classical and Quantum Gravity*, **36**, 105011

Rodriguez C. L., Zevin M., Amaro-Seoane P., Chatterjee S., Kremer K., Rasio F. A., Ye C. S., 2019, *Phys. Rev. D*, **100**, 043027

Rose S. C., Naoz S., Sari R., Linial I., 2022, *ApJ*, **929**, L22

Ruan W.-H., Guo Z.-K., Cai R.-G., Zhang Y.-Z., 2020, *International Journal of Modern Physics A*, **35**, 2050075

Sakurai Y., Yoshida N., Fujii M. S., Hirano S., 2017, *MNRAS*, **472**, 1677

Salpeter E. E., 1955, *ApJ*, **121**, 161

Sana H., et al., 2012, *Science*, **337**, 444

Shih D. C., Iwasawa K., Fabian A. C., 2003, *MNRAS*, **341**, 973

Skinner D., Wise J. H., 2020, *MNRAS*, **492**, 4386

Spera M., Mapelli M., 2017, *MNRAS*, **470**, 4739

Spitzer L., 1987, *Dynamical evolution of globular clusters*

Stacy A., Bromm V., Lee A. T., 2016, *MNRAS*, **462**, 1307

Strickland D. K., Colbert E. J. M., Heckman T. M., Weaver K. A., Dahlem M., Stevens I. R., 2001, *ApJ*, **560**, 707

Strohmayer T. E., Mushotzky R. F., 2009, *ApJ*, **703**, 1386

Sutton A. D., Roberts T. P., Walton D. J., Gladstone J. C., Scott A. E., 2012, *MNRAS*, **423**, 1154

Tagawa H., Kocsis B., Haiman Z., Bartos I., Omukai K., Samsing J., 2021, *ApJ*, **908**, 194

Takahashi K., Yoshida T., Umeda H., Sumiyoshi K., Yamada S., 2016, *MNRAS*, **456**, 1320

Takahashi K., Yoshida T., Umeda H., 2018, *ApJ*, **857**, 111

Takahashi K., Sumiyoshi K., Yamada S., Umeda H., Yoshida T., 2019, *ApJ*, **871**, 153

Taniguchi Y., Shioya Y., Tsuru T. G., Ikeuchi S., 2000, *PASJ*, **52**, 533

Tanikawa A., Yoshida T., Kinugawa T., Takahashi K., Umeda H., 2020, *MNRAS*, **495**, 4170

Tanikawa A., Kinugawa T., Yoshida T., Hijikawa K., Umeda H., 2021a, *MNRAS*, **505**, 2170

Tanikawa A., Susa H., Yoshida T., Trani A. A., Kinugawa T., 2021b, *ApJ*, **910**, 30

Tanikawa A., Yoshida T., Kinugawa T., Trani A. A., Hosokawa T., Susa H., Omukai K., 2022, *ApJ*, **926**, 83

The LIGO Scientific Collaboration the Virgo Collaboration the KAGRA Collaboration 2021, *arXiv e-prints*, p. [arXiv:2105.15120](https://arxiv.org/abs/2105.15120)

Totani T., Morokuma T., Oda T., Doi M., Yasuda N., 2008, *PASJ*, **60**, 1327

Tremou E., et al., 2018, *ApJ*, **862**, 16

Vierdayanti K., Mineshige S., Ebisawa K., Kawaguchi T., 2006, *PASJ*, **58**, 915

Wang H.-T., et al., 2019, *Phys. Rev. D*, **100**, 043003

Wang L., Nitadori K., Makino J., 2020a, *MNRAS*, **493**, 3398

Wang L., Iwasawa M., Nitadori K., Makino J., 2020b, *MNRAS*, **497**, 536

Wang L., Fujii M. S., Tanikawa A., 2021, *MNRAS*, **504**, 5778

Wang L., Tanikawa A., Fujii M. S., 2022, *MNRAS*, **509**, 4713

Webb N., et al., 2012, *Science*, **337**, 554

Wechsler R. H., Bullock J. S., Primack J. R., Kravtsov A. V., Dekel A., 2002, *ApJ*, **568**, 52

Wen L., 2003, *ApJ*, **598**, 419

Wiersema K., Farrell S. A., Webb N. A., Servillat M., Maccarone T. J., Barret D., Godet O., 2010, *ApJ*, **721**, L102

Will C. M., 2004, *ApJ*, **611**, 1080

Woosley S. E., 2017, *ApJ*, **836**, 244

Yoshida T., Takiwaki T., Kotake K., Takahashi K., Nakamura K., Umeda H., 2019, *ApJ*, **881**, 16

Zhao D. H., Mo H. J., Jing Y. P., Börner G., 2003, *MNRAS*, **339**, 12

Zocchi A., Gieles M., Hénault-Brunet V., 2017, *MNRAS*, **468**, 4429

van der Marel R. P., Gerssen J., Guhathakurta P., Peterson R. C., Gebhardt K., 2002, *AJ*, **124**, 3255

This paper has been typeset from a $\text{\TeX}/\text{\LaTeX}$ file prepared by the author.